

AD-A055 229

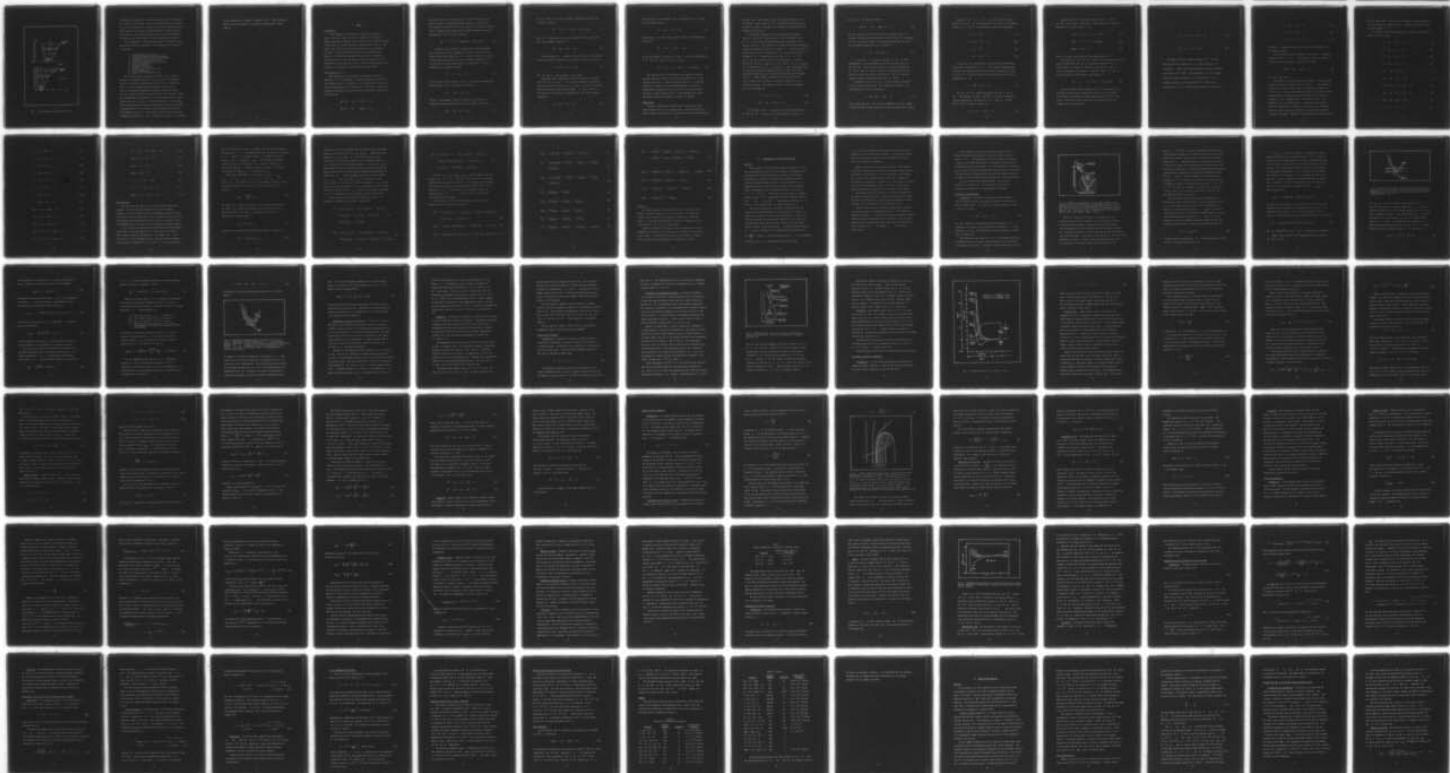
AIR FORCE INST OF TECH WRIGHT-PATTERSON AFB OHIO SCH--ETC F/G 20/5
REACTION-R CONSTANTS AND SIMPLE RATE THEORIES APPLIED TO THE ME--ETC(U)
MAR 78 R P SUMMERS

UNCLASSIFIED

AFIT/6NE/PH/78M-9

NL

1 of 2
AD
A055 229



AD A U 55229

FOR FURTHER TRAN

1



DDC
JUN 19 1978
E

UNITED STATES AIR FORCE
AIR UNIVERSITY

AIR FORCE INSTITUTE OF TECHNOLOGY
Wright-Patterson Air Force Base, Ohio

DDC FILE COPY

78 06 13 046

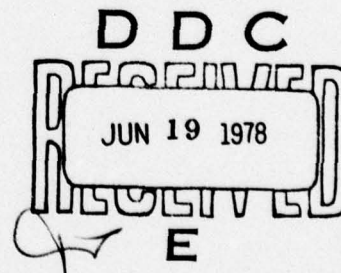
AFIT/GNE/PH/78M-9

REACTION-RATE CONSTANTS AND
SIMPLE RATE THEORIES APPLIED
TO THE MERCURY-CHLORIDE LASER

THESIS

AFIT/GNE/PH/78M-9

Robert P. Summers
Capt USAF



Approved for public release; distribution unlimited.

78 06 13 046

AFIT/GNE/PH/78M-9

REACTION-RATE CONSTANTS AND SIMPLE RATE THEORIES
APPLIED TO THE MERCURY-CHLORIDE LASER

THESIS

Presented to the Faculty of the School of Engineering
of the Air Force Institute of Technology
Air University
in Partial Fulfillment of the
Requirements for the Degree of
Master of Science

ACCESSION for		
NTIS	White Section	<input checked="" type="checkbox"/>
DDC	Buff Section	<input type="checkbox"/>
UNANNOUNCED		<input type="checkbox"/>
JUSTIFICATION.....		
BY.....		
DISTRIBUTION/AVAILABILITY CODES		
Dist.	AVAIL. and/or SPECIAL	
A		

by

Robert P. Summers, B.S.

Capt USAF

Graduate Nuclear Effects

March 1978

Approved for public release; distribution unlimited.

Preface

Developments in high-energy laser candidates are occurring at a rapid pace. As the number of candidates for the Department of Defense High-Energy Laser Program increases, an evaluation of each candidate in detail is more difficult. Therefore, the need for simple analyses of the candidates exists. These evaluations need to give approximate results for each laser so that research can be directed toward the more promising prospects.

This paper is an attempt to make a simple analysis of the HgCl laser which is a new candidate for the Department of Defense High-Energy Laser Program. Several of the reaction-rate constants for the reactions in the HgCl laser are computed by using simple theories applicable to these reactions. Some reaction-rate constants are computed by using experimental data. The model that is constructed from the reactions and reaction-rate constants is analyzed by both an analytical solution and a computer program solution.

Several people have provided me with assistance and aid throughout this study. Without the contact I have had with these people, this study would lack some key elements. In particular, I want to thank Dr. M. R. Flannery of the Joint Institute for Laboratory Astrophysics, Boulder, Colorado, for sending me copies of his calculated data on Hg^+ and Cl^- ionic recombination. I want to thank Dr. L. Schlie of the Air Force Weapons Laboratory for several interesting conversations. A great debt of gratitude is owed to A. M. Hunter of the AFIT Physics Department, my thesis advisor, for the invaluable help he gave me throughout my research. I want to thank Ms. Sharon Flores for typing the final copy of this thesis. Finally, a special note of thanks to my wife, Kathy, for her patience and many hours spent typing the rough draft of this thesis.

Contents

	<u>Page</u>
Preface.....	ii
List of Figures.....	v
List of Tables.....	vi
Abstract.....	vii
I. Introduction.....	1
II. Model.....	7
Introduction.....	7
Eden's Analysis.....	7
Simple Model.....	10
Rate Equations.....	19
Conclusion.....	24
III. Reaction-Rate Constants and Theories.....	25
Overview.....	25
Dissociative Recombination.....	26
Introduction.....	26
Theory.....	27
Experimental Values and Calculations.....	35
Conclusion.....	36
Dissociative Attachment.....	37
Introduction.....	37
Theoretical and Experimental Results.....	38
Conclusion.....	40
Ion-Neutral Association Reactions.....	40
Introduction.....	40
Mahan's Theory.....	42
Smirnov's Theory.....	46
Conclusion.....	50
Charge Transfer Reactions.....	52
Introduction.....	52
Gioumousis and Stevenson's Theory.....	52
Rapp and Francis' Theory.....	55
Experimental Data.....	56
Conclusion.....	58
Ion-Ion Recombination.....	58
Introduction.....	58
Thomson's Theory.....	59
Langevin's Theory.....	64
Natanson's Theory.....	65
Wadehra and Bardsley's Theory.....	65
Conclusion.....	65

Harpooning and Similar Reactions.....	67
Introduction.....	67
Theory.....	68
Experimental Work.....	69
Conclusion.....	70
Secondary-Electron Excitation of Ar, Xe, and Hg...	71
Introduction.....	71
Ar and Xe.....	72
Hg.....	73
Conclusion.....	74
Ionization of Excited States by Secondary-	
Electron Impact.....	74
Introduction.....	74
Ar*, Xe*, and Hg*.....	75
Conclusions.....	76
Cl-Cl Recombination Reactions.....	77
Radiative Decay of ArCl*, XeCl*, and HgCl*.....	78
Ionization and Excitation by Electron Beam.....	79
HgCl* Quenching.....	79
Summary.....	80
IV. Solution and Analysis.....	83
Overview.....	83
Slow Varying Species.....	84
Solution for HgCl Laser Without Applied	
Electric Field.....	86
Introduction and Assumptions.....	86
Analytical Solution.....	87
Conclusion.....	90
Solution for the HgCl Laser With Applied	
Electric Field.....	91
Introduction and Assumptions.....	91
Analytical Solution.....	92
Conclusion.....	96
Summary.....	96
V. Conclusions and Recommendations.....	97
References.....	100
Appendix A: Other Possible Reactions in HgCl Laser.....	104
Appendix B: Photodetachment of Cl ⁻	105
Appendix C: M. R. Flannery's Ionic Recombination Curves.....	106
Vita.....	108

List of Figures

<u>Figure</u>		<u>Page</u>
1	Oscillogram of Typical HgCl ($B \rightarrow X$) Fluorescence	2
2	HgCl Potential Energy Curves	4
3	Potential Energy Curves for Direct Dissociative Recombination	28
4	Hypothetical Potential Energy Curves and Wave Functions for Direct Dissociative Recombination	31
5	Hypothetical Potential Energy Curves for Indirect Dissociative Recombination	34
6	Potential Energy Curves and Nuclear Wave Functions in Dissociative Attachment	39
7	Potential Energy Curves for Cl_2 and Cl_2^-	41
8	Typical Family of Trajectories as a Function of the Impact Parameter	54
9	Potential Energy Curves for an Alkali Halide Molecule	69
10	Hg^+ and Cl^- Ionic Recombination Constants for Pressures to 3 Atmospheres	106
11	Hg^+ and Cl^- Ionic Recombination Constants	107

List of Tables

<u>Table</u>		<u>Page</u>
I	Ion-Ion Recombination Constants for the HgCl Laser	67
II	Reactions and Reaction-Rate Constants	80
III	Equilibrium n_e as a Function of n_{cl} -	90
IV	Equilibrium n_e as a Function of Electron Beam Current	90
V	Computer Solution for HgCl Laser and R_{9a} Varied	95
VI	Computer Solution for HgCl Laser and Electron Beam Current Varied	95

Abstract

Several simple theories for reaction-rate constants are applied to the HgCl (Mercury-Chloride) laser reactions. These theories are discussed and analyzed using existing data. The theories that are discussed are applicable to dissociative recombination, dissociative attachment, ion neutral association, bimolecular charge transfer reactions, ionic recombination, and harpooning reactions.

A simple theoretical model of the HgCl laser is constructed. The gases that are included in the laser are Ar, Xe, Hg, and Cl₂. Reaction-rate constants for the reactions are computed using either theoretical or experimental data. The model is analyzed using an analytical approach and a computer generated solution. The model is found to be very sensitive to the dissociative attachment rate of Cl₂ and electron impact pumping rate constants.

REACTION-RATE CONSTANTS AND SIMPLE RATE THEORIES APPLIED TO THE MERCURY-CHLORIDE LASER

I. Introduction

Developments in high-energy lasers sometimes come faster than the reaction-rate-constant experimental data necessary to analyze these lasers. For example, both the KrF and HgCl lasers are candidates for the Department of Defense High-Energy Laser Program. Yet, no complete analyses of their reaction kinetics exist to determine their scalability to larger than a laboratory model. These analyses do not exist, because experimental data is not complete on all the major reactions to determine their reaction-rate constants.

As more potential high-energy lasers are developed, the need to determine reaction-rate constants increases. Two approaches can be taken to solve this expanding problem. One method to determine which reaction-rate constants are most important to the reaction kinetics of a laser is to experimentally determine all the possible reaction-rate constants. A second method is to determine theoretically all the contributing reaction-rate constants. Neither method is totally satisfactory, because of the time that is required to do each in detail.

A better method to determine the important reaction-rate constants is to do simple theoretical calculations to determine an order-of-magnitude for the reaction rates. After the important contributing reactions to the laser are theoretically determined, experiments can

be conducted to verify that these reactions are important and to determine the exact reaction-rate constants for these reactions. In this paper, simple theories and theoretical calculations are reported for the HgCl laser reaction kinetics.

Both Parks (Ref 1) and Eden (Ref 2) report observing lasing in a mercury-chloride laser at a wavelength of 5576 \AA . The lasing is achieved by electron-beam pumping of mixtures of Ar, Xe, Hg, and CCl_4 . Eden reports that double line laser oscillation is achieved at 5576.2 \AA and 5583.5 \AA with a mixture of 85% Ar, 11% Xe, 4% Hg, and 0.2% CCl_4 (Ref 2). An oscillogram of one of Eden's HgCl laser actions with a single laser oscillation at 5576.2 \AA is given in his article and is shown in Figure 1.

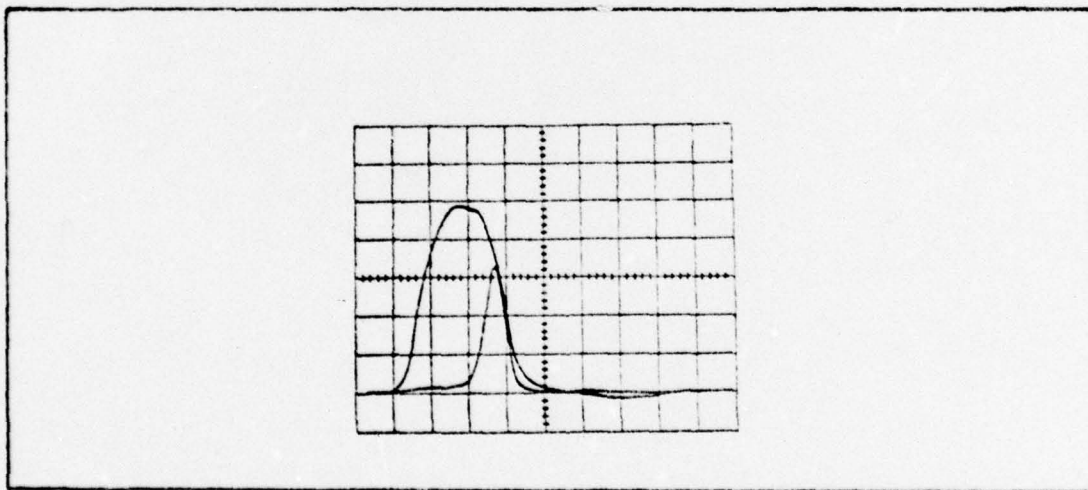


Fig. 1. Oscillogram of typical HgCl(B-X) fluorescence (upper trace) and laser emission waveforms for a mixture of 85.4% Ar/10.4% Xe/4.0% Hg/0.2% CCl_4 , pressure = 3.43 atmospheres, $T_{\text{cell}} = 304^\circ\text{C}$, and $T_{\text{reservoir}} = 260^\circ\text{C}$. Horizontal scale: 20 ns/div; vertical units arbitrary (Ref 2).

Three characteristics of the HgCl laser make it an excellent candidate for a high-energy laser. First, the wavelength of the HgCl laser is 5576 Å which is in the blue-green portion of the spectrum. Laser light in the visible range is attributed with better atmospheric propagation characteristics than laser action with a longer wavelength such as the CO₂ laser at 10.6 microns. Problems such as atmospheric absorption, aerosol absorption and scattering, thermal blooming, and wind turbulence are greater limiting factors on lasers with a longer wavelength (Ref 3). Because it lases in the visible part of the spectrum, the capability exists for the HgCl laser to be used during a greater variety of atmospheric conditions. Second, the potential quantum efficiency of the HgCl laser is 45% if it is pumped by a discharge (Ref 1). Obviously, this high quantum efficiency makes the entire system more efficient. Third, the energy per photon of the HgCl laser is higher than for a laser with a longer wavelength.

The HgCl potential energy curves are shown in Figure 2.

Before the HgCl laser can be exploited as a high-energy laser, a detailed analysis of the HgCl laser reaction kinetics must be completed. The theories and calculated theoretical values that are reported in this paper provide some information toward determining which reactions are important in the HgCl laser.

The approach taken to analyze the HgCl laser in this paper is a three step approach. First, a simple model of the reaction kinetics for the HgCl laser is constructed using Eden's analysis (Ref 2) as a guide. Second, simple theories are investigated for the various reactions, and theoretical calculations are made to determine the important reaction-rate constants. These theoretical

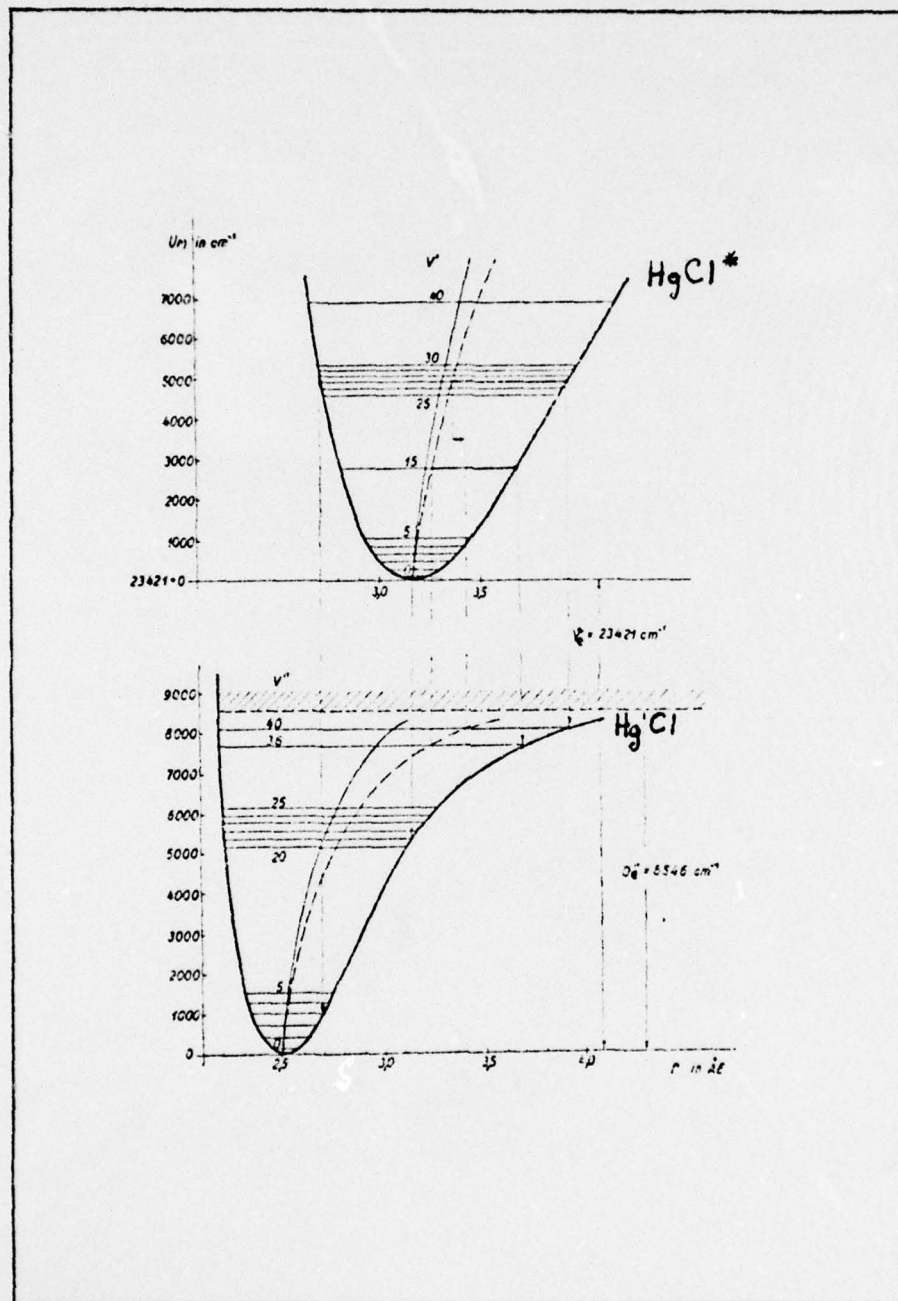


Fig. 2. HgCl Potential Energy Curves (Ref 4)

calculations are compared to available experimental data to determine the validity of the theories. Third, the rate equations of the model are solved and subjected to a sensitivity analysis to further determine which reaction-rate constants need more research. During the sensitivity analysis, reaction-rate constants are varied to determine the sensitivity of the entire model to a given reaction-rate constant.

The investigation of reaction-rate constants is limited to those applicable to the HgCl laser model. The following type of reactions are included:

1. ionization by electron impact
2. electron-ion dissociative recombination
3. electron-molecule dissociative attachment
4. ion-neutral association reactions
5. bimolecular charge transfer reactions
6. ion-ion recombination
7. "harpoon" reactions
8. excitation by electrons
9. radiative decay of excited atoms
10. Cl-Cl recombination
11. quenching of excited HgCl by Cl₂

The following general assumptions are made. First, classical mechanics and quantum mechanics are valid. Second, colliding heavy particles follow the trajectories predicted by classical mechanics. Third, the energy transitions of the internal states of heavy particles calculated using quantum mechanical perturbation theory are valid. Heavy particles are particles other than electrons. Fourth, the perturbed Hamiltonian determined by the time-dependent collisional interaction using a classical collision model applies to this problem. Fifth, the electron energy distribution and the gas energy distribution are Maxwellian and are at different average energies of 4eV (Ref 5) and 0.0689eV, respectively. The assumption that the electrons are in a Maxwellian distribution is made to simplify calculations. The validity

of this assumption is discussed in Chapters 4 and 5. Other assumptions made for individual theories are stated in the discussion of those theories.

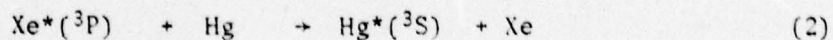
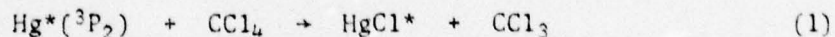
II. Model

Introduction

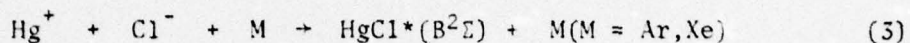
In this chapter, a simple model is developed for the HgCl laser. This simple model is used as a guide for investigation of specific reactions in the HgCl laser. The first step in the development of this model is a brief discussion of Eden's analysis (Ref 2). The second step is the selection of the reactions that are included in the model. Some of the reactions that are not included in this model, yet can affect the lasing action, are listed in Appendix A. The third step is to list the rate or continuity equations for each species that is involved in this model. Some concluding remarks about the model are included as the last section of this chapter.

Eden's Analysis (Ref 2)

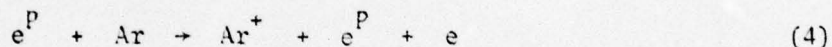
Eden reports that his experiments were conducted primarily at pressures of 2 to 5 atmospheres. At these high pressures, Eden states that harpoon reaction in equation 1 is not significant. The harpoon reaction creating the HgCl* in reaction 1 is the result of outer shell electrons rearranging to form an attractive bond between the Hg* atom and the Cl atom.



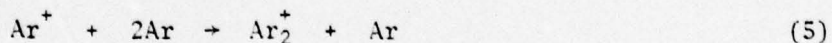
The small cross section for reaction 2, $\sigma \leq 10^{-3} \text{ \AA}^2$ limits the Hg^* that is created to insignificant number densities. This lack of Hg^* necessary for reaction 1 makes this mode of HgCl^* formation insignificant. Therefore, the primary mode for HgCl^* formation is the ionic recombination of Hg^+ and Cl^- by reaction 3.



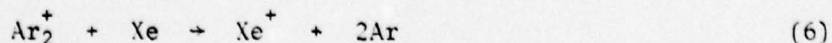
According to Eden, the Hg^+ is produced in the following manner. The electron beam energy is absorbed by the Ar to create Ar^+ by the electron-impact ionization of Ar. This reaction is shown in reaction 4. A high energy beam electron or primary electron is indicated by e^P . An electron other than a beam electron is indicated by e and is referred to as a secondary electron.



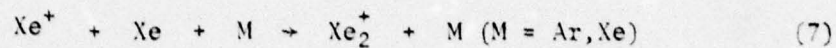
The Ar^+ reacts with two other Ar atoms in an ion-neutral recombination reaction to get Ar_2^+ , and is shown in reaction 5.



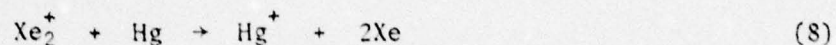
The Ar_2^+ then transfers a positive charge to a Xe atom in the bimolecular charge transfer reaction that is shown in reaction 6.



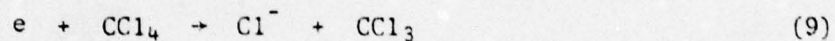
The Xe^+ forms Xe_2^+ by the ion-neutral recombination reaction that is shown in reaction 7.



The Hg^+ is created by the bimolecular charge transfer reaction with Xe_2^+ that is shown in reaction 8.



The only mode of Cl^- creation in Eden's analysis is the electron-molecule dissociative-attachment reaction that is shown in reaction 9.



The Hg^+ and Cl^- then recombine to form HgCl^+ .

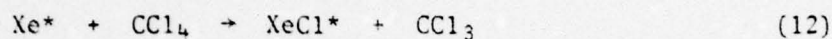
Eden notes that a fluorescence at 3080 Å indicates a transition from $\text{XeCl}^*(\text{B})$ to $\text{XeCl}(\text{X})$. This transition indicates a competing chain of reactions for the use of Cl^- exists. The chain of competing reactions develops in the following manner. The first reaction is the electron-ion dissociative recombination of Ar_2^+ that is shown in reaction 10.



The excitation of the metastable Ar^* is transferred to a Xe atom by the two-body reaction 11.



The metastable Xe^* then creates excited XeCl^* by the harpoon-like reaction 12.



An alternate method of formation for XeCl^* is the ionic recombination of Xe^+ and Cl^- that is shown in reaction 13.



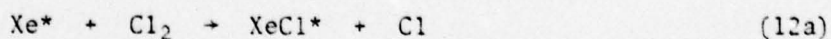
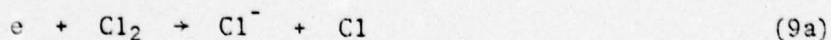
This reaction scheme of contributing and competing reactions indicates the need to know the reaction-rate constants for all the reactions that exist. A simple analytical analysis of all possible reactions is impossible in a time-dependent model. Therefore, a simple model is constructed to analyze some of the reactions that are given in Eden's analysis (Ref 2). Some reactions that are not considered by Eden are included in the model for analysis.

Simple Model

The model constructed in this section is developed by using Eden's analysis (Ref 2) as a starting point. Several reactions are added to Eden's analysis (Ref 2) to emphasize specific points concerning

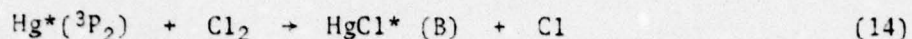
the HgCl laser. Most of Eden's analysis for high pressures (Ref 2) is included. Eden's source of Xe^* is modified and explained later. Therefore, reactions 3 through 13 are included in this model with the exception of reaction 11.

In this model, reactions 9 and 12 are modified from Eden's analysis. Eden (Ref 2) and Parks (Ref 1) state that their source of Cl^- was the electron-molecule dissociative attachment of CCl_4 shown in reaction 9. This model uses the same type of electron-molecule dissociative attachment reaction to create Cl^- . The source molecule chosen for this model is changed from CCl_4 that is used by Parks and Eden to Cl_2 , because the cross section of Cl_2 is 90 \AA^2 (Ref 6) for the harpoon reaction that is investigated. The cross section for the CCl_4 reaction is 34 \AA^2 (Ref 6). The Cl_2 molecule is also substituted for CCl_4 in reaction 12. This slight change does not present any theoretical problems, but this change may create experimental problems due to the health hazards and corrosive nature of Cl_2 . Eden's comment concerning the slow attacking on his cavity windows (Ref 2) indicates a potential problem with any Cl atom creating chain. The modified reactions 9 and 12 are numbered 9a and 12a, respectively.

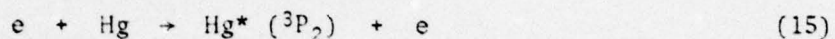


In this model, HgCl^* is created by the ion-ion recombination of Hg^+ and Cl^- in reaction 3 and the harpooning reaction with

Hg* and Cl₂ in reaction 14 (Ref 6).

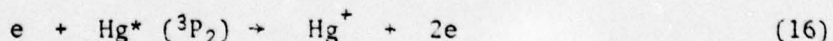


The Hg* necessary for reaction 14 is not created by reaction 2 because of the small cross section for transfer of the Xe* excitation to Hg* in reaction 2 (Ref 2). The alternate method that is used is the electronic excitation of Hg in reaction 15.



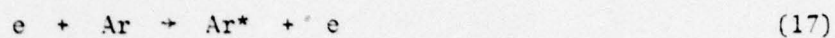
Only Hg* (³P₂) is considered, because Hg* (³P₂) is found experimentally to be the dominant mercury atom to react with Cl₂. The Hg* (³P₀) reaction cross section for a harpoon reaction with Cl₂ to the HgCl*(B) state is found to be one-fifth the Hg* (³P₂) reactive cross section for the same reaction. Hg* (³P₁) does not appear to create a chemiluminescence with Cl₂ (Ref 6).

The possible loss of Hg* (³P₂) by electron-impact ionization is also included in this model. This reaction is a source of Hg⁺ and electrons as is seen in reaction 16.



For the remaining text, Hg* is used to symbolize Hg* (³P₂) unless a distinction must be made between the various excited states of mercury.

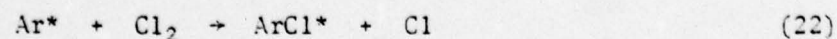
Sources of Ar^* , Xe^* , Ar^+ , and Xe^+ similar to those listed for Hg^* and Hg^+ are considered in this model. The following reactions of Ar and Xe with secondary electrons are considered.



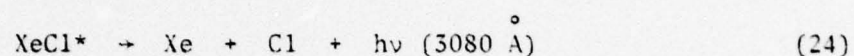
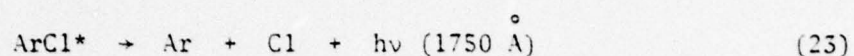
A source of Xe^* not mentioned by Eden is the electron-molecule dissociative recombination of Xe_2^+ . This reaction is theoretically the same as the electron-molecule dissociative recombination of Ar_2^+ in reaction 10. Reaction 21 shows the electron-molecule dissociative recombination of Xe_2^+ .



The Ar^* and Xe^* provide competition with Hg^* for use of Cl_2 . The formation of HgCl^* and XeCl^* is shown in reactions 14 and 12a, respectively. The reaction of Ar^* with Cl_2 to form ArCl^* (Ref 7) is shown in reaction 22.



Possible effects of the radiative decay of ArCl^* , XeCl^* , and HgCl^* are included in this model. These reactions are shown in reactions 23, 24, and 25 (Refs 2, 7, 8).

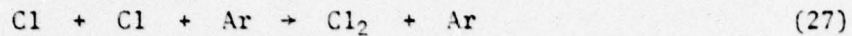


Reactions 23 and 24 are bound-free type transitions (Ref 7).

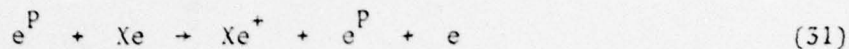
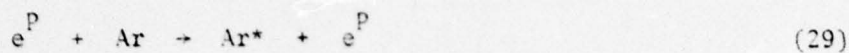
The existence of Ar^+ and Xe^+ created in several reactions indicates possible competition with Hg^+ for neutralizing reactions with Cl^- atoms created in reaction 9a. Reaction 13 shows the Xe^+ and Cl^- ion-ion recombination in reaction 3. Reaction 26 shows Ar^+ and Cl^- ion-ion recombination and competes with reaction 3.



Several reactions create a neutral Cl atom. Two reactions for the three-body neutral-neutral recombination of Cl to Cl_2 are included in the model to investigate the impact they have on the overall laser action. Reactions 27 and 28, which were investigated by Clyne and Stedman (Ref 9) are shown here.

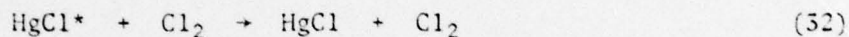


Eden (Ref 2) shows the primary electrons, e^P , for the electron beam only reacting with Ar in the creation of Ar^+ in reaction 4. Three other reactions using the primary electrons are included in this model. The excitation of Ar by a primary electron is shown in reaction 29. The excitation of Xe by a primary electron is shown in reaction 30. Finally, the ionization of Xe by a primary electron is shown in reaction 31.



The symbol e represents the ionized electron and is referred to as a secondary electron.

The final reaction that is included in this model is a quenching reaction of $HgCl^*$ by Cl_2 . This reaction is shown in reaction 32. In this reaction, the $HgCl^*$ is quenched to a bound

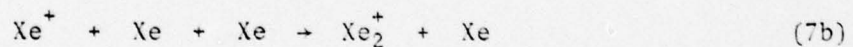
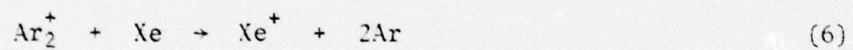
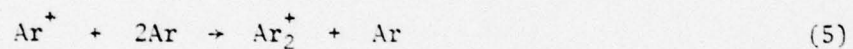
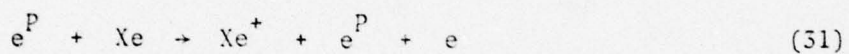
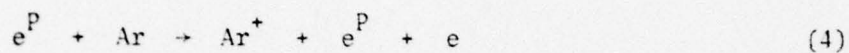


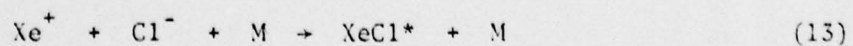
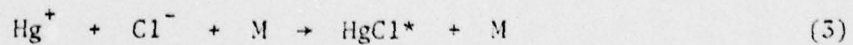
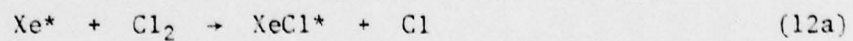
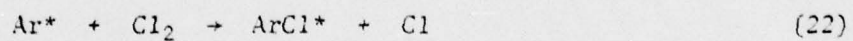
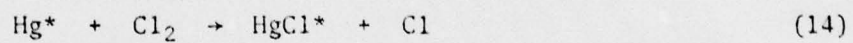
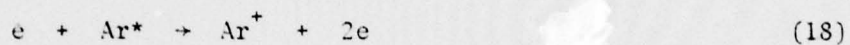
state for $HgCl$ (Ref 8).

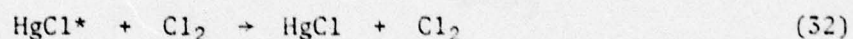
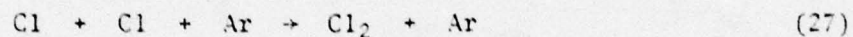
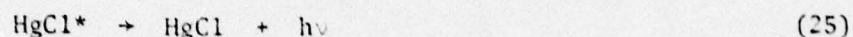
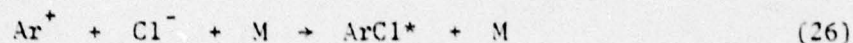
Several facts are interesting about this model. First, the model does not include the radiative decay of $Hg^*(^3P_2)$. This radiative lifetime is extremely long and results in a transition probability of 10^{-1} sec^{-1} (Ref 10) which should not affect this problem. Second, the model does not include the possible existence of a stabilized molecule of Cl_2^- at higher operating pressures (Ref 11). This molecular ion is a possible source of several types of reactions. Third, the model does not include a loss term for $HgCl$ molecules. This fact creates some minor problems in the analytical equilibrium solution of the model. Essentially, no true equilibrium solution exists

for this simple model, since at least one species is always increasing or always decreasing in number density. Appendix B explains the lack of photodetachment of Cl^- .

As a summary, the following reactions are included in this simple model of the HgCl laser.







Rate Equations

Each reaction in the model occurs with a specific reaction-rate constant. This reaction-rate constant multiplied by the number densities of the reacting species equals the number per cubic centimeter per second of a given species that is lost or created in a given reaction. Rate equations must be determined for each species in the model, so the interdependence of all the species can be resolved in the final solution.

In this section, rate equations are listed for all species included in the model. A specific species is any atom, molecule, or electron with a specific chemical characteristic. For example, Hg^+ , Hg , and $\text{Hg}^*(^3\text{P}_2)$ are all different species. The reaction-rate constants in this paper are symbolized by R_i , where i is the reaction number

used in the previous sections. For example, the reaction-rate constant for reaction 4 is R_4 . The number density for each species is indicated by n_A , where A is a specific species. For example, the number density of Hg^* is indicated by n_{Hg^*} . The time-rate of change of a specific species is indicated by \dot{n}_A , where \dot{n} indicates the differential $\frac{dn}{dt}$ and A indicates a specific species. For example, the time-rate of change of Cl^- is indicated by \dot{n}_{Cl^-} .

Other symbols introduced in this section are S_{Ar^+} , j_{eb} , n_{eb} , v_{eb} , q_e , σ_{Ar} , σ_{Xe} , σ_{*Ar} , and σ_{*Xe} . The symbol S_{Ar^+} is the number of Ar^+ ions or secondary electrons created per cubic centimeter per second by the incident electron beam in reaction 4.

$$S_{Ar^+} = \frac{j_{eb} \sigma_{Ar}}{q_e} n_{Ar} \quad (33)$$

The symbol j_{eb} indicates the current of the incident electron beam. The symbol n_{eb} represents the number density of beam electrons in the electron beam. The symbol v_{eb} represents the speed of a monoenergetic primary electron.

$$j_{eb} = q_e n_{eb} v_{eb} \quad (34)$$

Substitution of equation 34 into equation 33 results in equation 33a.

$$S_{Ar^+} = n_{eb} n_{Ar} v_{eb} \sigma_{Ar} \quad (33a)$$

Equation 33a is in a more standard rate of reaction form. The number densities of reacting species are n_{eb} and n_{Ar} . The reaction-rate constant is $\sigma_{Ar} v_{eb}$ where σ_{Ar} is the cross section for the ionization of Ar by primary electrons with a specific energy and v_{eb} is the speed of the approaching electron. In this case, v_{eb} is approximately the speed of approach of the two particles, because the speed of the electron is several orders-of-magnitude greater than the speed of the Ar. Similar arguments exist for the terms including σ_{Xe} , σ_{*Xe} , and σ_{*Ar} where σ_{Xe} is the cross section for ionization of Xe by a primary electron in reaction 31, σ_{*Xe} is the cross section for excitation of Xe to a metastable state by a primary electron in reaction 30, and σ_{*Ar} is the cross section for excitation of Ar to a metastable state by a primary electron in reaction 29.

The rate equations for secondary electrons, Ar, and Xe are presented in equations 35, 36, and 37, respectively.

$$\begin{aligned} \dot{n}_e = & v_{eb} \sigma_{Ar} n_{eb} n_{Ar} + v_{eb} \sigma_{Xe} n_{eb} n_{Xe} - R_{9a} n_e n_{Cl_2} \\ & + R_{16} n_e n_{Hg^*} + R_{18} n_e n_{Ar^*} + R_{20} n_e n_{Xe^*} \\ & - R_{10} n_e n_{Ar_2^+} - R_{21} n_e n_{Xe_2^+} \end{aligned} \quad (35)$$

$$\begin{aligned} \dot{n}_{Ar} = & -v_{eb} \sigma_{Ar} n_{eb} n_{Ar} - v_{eb} \sigma_{*Ar} n_{eb} n_{Ar} - R_5 n_{Ar^+} n_{Ar} \\ & + 2R_6 n_{Ar_2^+} n_{Xe} - R_{17} n_e n_{Ar} + R_{10} n_e n_{Ar_2^+} + R_{23} n_{ArCl^*} \end{aligned} \quad (36)$$

$$\begin{aligned}
\dot{n}_{\text{Xe}} = & -v_{\text{eb}} \sigma_{\text{Xe}} n_{\text{eb}} n_{\text{Xe}} - v_{\text{eb}} \sigma_{\text{Xe}} n_{\text{eb}} n_{\text{Xe}} - R_6 n_{\text{Ar}_2^+} n_{\text{Xe}} \\
& - (R_{7a} n_{\text{Ar}} + R_{7b} n_{\text{Xe}}) n_{\text{Xe}} n_{\text{Xe}^+} + 2R_8 n_{\text{Xe}_2^+} n_{\text{Hg}} \\
& - R_{19} n_e n_{\text{Xe}} + R_{21} n_e n_{\text{Xe}_2^+} + R_{24} n_{\text{XeCl}^*}
\end{aligned} \tag{37}$$

The term $(R_{7a} n_{\text{Ar}} + R_{7b} n_{\text{Xe}}) n_{\text{Xe}} n_{\text{Xe}^+}$ that is found in the rate equations for Xe , Xe^+ , and Xe_2^+ is the sum of the two possible contributions from reactions 7a and 7b to these specific rate equations. This term is the result of two possible third reacting bodies in the formation of Xe_2^+ . The third body is not included in the ionic recombination of Ar^+ , Xe^+ , and Hg^+ with Cl^- for reasons that are discussed in Chapter 3.

The rate equations for the remaining species involved in the model are listed in Equations 58 through 53.

$$\begin{aligned}
\dot{n}_{\text{Xe}^+} = & v_{\text{eb}} \sigma_{\text{Xe}} n_{\text{eb}} n_{\text{Xe}} + R_6 n_{\text{Ar}_2^+} n_{\text{Xe}} - (R_{7a} n_{\text{Ar}} + R_{7b} n_{\text{Xe}}) n_{\text{Xe}} n_{\text{Xe}^+} \\
& + R_{20} n_e n_{\text{Xe}^*} - R_{13} n_{\text{Xe}^+} n_{\text{Cl}^-}
\end{aligned} \tag{38}$$

$$\dot{n}_{\text{Xe}_2^+} = (R_{7a} n_{\text{Ar}} + R_{7b} n_{\text{Xe}}) n_{\text{Xe}} n_{\text{Xe}^+} - R_8 n_{\text{Xe}_2^+} n_{\text{Hg}} - R_{21} n_e n_{\text{Xe}_2^+} \tag{39}$$

$$\dot{n}_{\text{Ar}^+} = v_{\text{eb}} \sigma_{\text{Ar}} n_{\text{eb}} n_{\text{Ar}} - R_5 n_{\text{Ar}^+} n_{\text{Ar}}^2 + R_{18} n_e n_{\text{Ar}^*} - R_{25} n_{\text{Ar}^+} n_{\text{Cl}^-} \tag{40}$$

$$\dot{n}_{Ar_2^+} = R_5 n_{Ar^+} n_{Ar}^2 - R_6 n_{Ar_2^+} n_{Xe} - R_{10} n_e n_{Ar_2^+} \quad (41)$$

$$\begin{aligned} \dot{n}_{Ar^*} = & v_{eb} \sigma_{Ar} n_{eb} n_{Ar} + R_{17} n_e n_{Ar} - R_{18} n_e n_{Ar^*} + R_{10} n_e n_{Ar_2^+} \\ & - R_{22} n_{Ar^*} n_{Cl_2} \end{aligned} \quad (42)$$

$$\begin{aligned} \dot{n}_{Xe^*} = & v_{eb} \sigma_{Xe} n_{eb} n_{Xe} + R_{19} n_e n_{Xe} - R_{20} n_e n_{Xe^*} + R_{21} n_e n_{Xe_2^+} \\ & - R_{12a} n_{Xe^*} n_{Cl_2} \end{aligned} \quad (43)$$

$$\dot{n}_{Hg} = -R_8 n_{Xe_2^+} n_{Hg} - R_{15} n_e n_{Hg} \quad (44)$$

$$\dot{n}_{Hg^+} = R_8 n_{Xe_2^+} n_{Hg} + R_{16} n_e n_{Hg^*} - R_5 n_{Hg^+} n_{Cl^-} \quad (45)$$

$$\dot{n}_{Hg^*} = R_{15} n_e n_{Hg} - R_{16} n_e n_{Hg^*} - R_{14} n_{Hg^*} n_{Cl_2} \quad (46)$$

$$\dot{n}_{Cl_2} = -R_{9a} n_e n_{Cl_2} + R_{28} n_{Cl}^2 n_{Cl_2} + R_{27} n_{Cl}^2 n_{Ar} \quad (47)$$

$$\dot{n}_{Cl^-} = R_{9a} n_e n_{Cl_2} - R_5 n_{Hg^+} n_{Cl^-} - R_{15} n_{Xe^+} n_{Cl^-} - R_{26} n_{Ar^+} n_{Cl^-} \quad (48)$$

$$\begin{aligned} \dot{n}_{Cl} = & R_{9a} n_e n_{Cl_2} + R_{14} n_{Hg^*} n_{Cl_2} + R_{22} n_{Ar^*} n_{Cl_2} + R_{12a} n_{Xe^*} n_{Cl_2} \\ & + R_{23} n_{ArCl^*} + R_{24} n_{XeCl^*} - R_{28} n_{Cl}^2 n_{Cl_2} - R_{27} n_{Cl}^2 n_{Ar} \end{aligned} \quad (49)$$

$$\dot{n}_{HgCl^*} = R_{14} n_{Hg^*} n_{Cl_2} + R_3 n_{Hg^+} n_{Cl^-} - R_{32} n_{HgCl^*} n_{Cl_2} - R_{25} n_{HgCl^*} \quad (50)$$

$$\dot{n}_{ArCl^*} = R_{22} n_{Ar^*} n_{Cl_2} + R_{26} n_{Ar^+} n_{Cl^-} - R_{23} n_{ArCl^*} \quad (51)$$

$$\dot{n}_{XeCl^*} = R_{12a} n_{Xe^*} n_{Cl_2} + R_{15} n_{Xe^+} n_{Cl^-} - R_{24} n_{XeCl^*} \quad (52)$$

$$\dot{n}_{HgCl} = R_{32} n_{HgCl^*} n_{Cl_2} + R_{25} n_{HgCl^*} \quad (53)$$

Conclusion

The simple model that is presented here does not include all the possible reactions taking place in the HgCl laser. This model does include several reactions not considered by Parks (Ref 1) and Eden (Ref 2). A major deviation from Parks' and Eden's experiments is the substitution of Cl_2 for CCl_4 in the model.

Before any solution can be found for the rate equations that are presented in this section, the reaction-rate constants for each reaction must be found. The reaction-rate constants are developed in Chapter 3, and a solution for the rate equations is presented in Chapter 4.

III. Reaction-Rate Constants and Theories

Overview

In this chapter, the reaction-rate constants necessary to solve the rate equations in Chapter 2 are developed. The processes that are discussed and include theoretical sections are dissociative recombination, dissociative attachment, ion-neutral association reactions, charge transfer reactions, ion-ion recombination, and harpooning reactions. Reaction-rate constants that are presented based on experimental data are secondary-electron excitation of Ar , Xe , and Hg , ionization of excited states by secondary-electron impact, Cl-Cl recombination reactions, radiative decay of ArCl* , XeCl* , and HgCl* , ionization and excitation of Ar and Xe by the electron beam, and HgCl* quenching by Cl₂ .

Some of the reaction-rate constants for these processes are the result of direct measurement of the reaction-rate constant, and others are the result of cross section measurements. If only cross sections are found, the reaction-rate constant for that process can be calculated by multiplying the cross section times the average relative velocity of the two particles. The average relative velocity, v_r , is found for particles in a Maxwell-Boltzmann distribution to be $(\frac{8kT}{\pi M_r})^{1/2}$ where k is the Boltzmann constant, T is the temperature of the gas, and M_r is the reduced mass of the particles.

17, 18) exist for dissociative recombination reactions and provide reasonable data for reaction-rate constants. This section includes summaries of applicable theoretical and experimental work that exist for dissociative recombination.

Theory. Dissociative recombination requires a free electron with positive energy to give away energy to become a bound electron with negative energy (Ref 12). This excess energy can be radiated away or given up in a collision with a third body. Dissociative recombination is essentially a two-body collision between an electron and a molecule containing two atoms. One of these atoms is the third body necessary to absorb the excess energy of the electron.

The electrons that are captured in dissociative recombination are thermal electrons (Ref 12). These electrons provide the energy necessary for molecular ions to form unstable intermediate neutral molecules AB'' that dissociate into two neutral atoms.

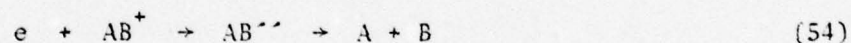
Figure 3 shows the shape of potential energy curves necessary for direct dissociative recombination to occur. The internuclear separation distance R_c is the point at which the energy the thermal electron provides for the reaction is sufficient to move the bound molecular ion to the higher potential energy curve of the unstable neutral molecule AB'' . This point, R_c , is called the capture point.

In this chapter, the electrons are still assumed to be in a Maxwell-Boltzmann distribution with an average energy of $\frac{3}{2} kT_e$ equal to 4 eV . This assumption is made to simplify calculations. A solution of the Boltzmann equation is required to find the actual distribution function of electrons. This new distribution is required to give correct answers for reaction-rate constants that are calculated for electron-impact excitation and ionization by secondary electrons. A solution of the Boltzmann equation is beyond the scope of this paper.

The next section of this paper contains a discussion of dissociative recombination. The reaction-rate constants for dissociative recombination are experimentally determined.

Dissociative Recombination

Introduction. Dissociative recombination is the reaction in which a diatomic molecular ion captures an electron and dissociates into two neutral atoms. This reaction is shown in reaction 54 where A and B are atoms.



The AB'' molecule is an intermediate unstable molecule. Two reactions in this model involve dissociative recombination. In these reactions, Ar_2^+ and Xe_2^+ dissociate to form the appropriate products shown in reaction 54.

The theoretical work (Refs 12, 13, 14, 15) concerning dissociative recombination does not provide simple formulas for quick calculation of reaction-rate constants. Fortunately, several experiments (Refs 16,

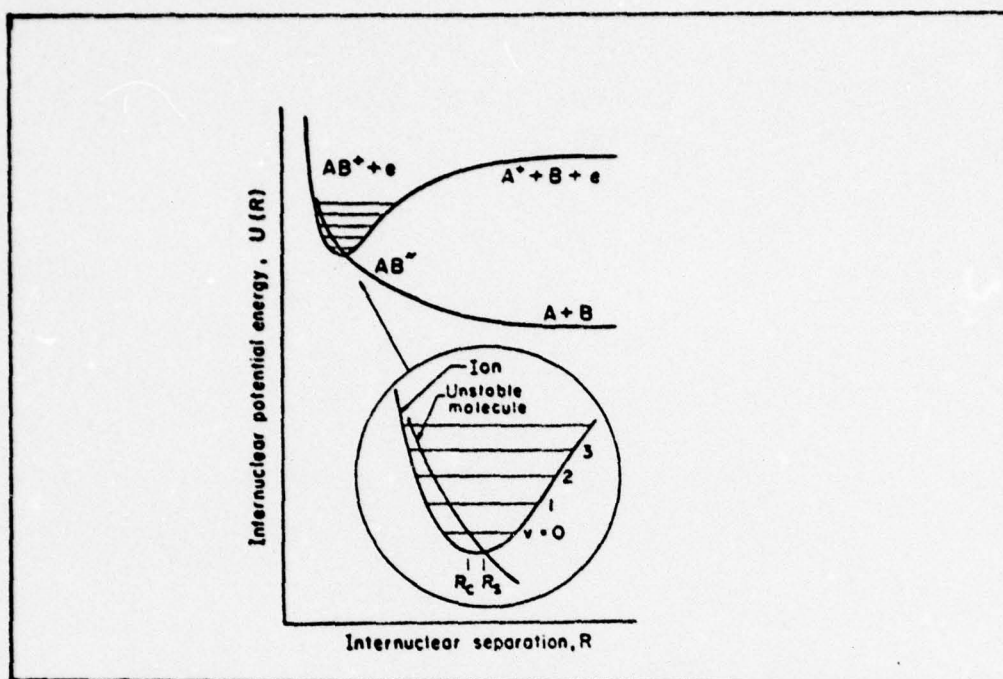


Fig. 3. Schematic representation of the potential energy curves involved in the direct dissociative recombination process. In this simplified example, only one potential curve for the molecular ion AB^+ (with an electron at rest at infinity) and one for the unstable molecule AB^- are shown. Inset: magnified view of the potential curves in the curve-crossing region. (Ref 12).

After the electron is attached by the molecular ion, two possibilities exist for the unstable molecule. The first possibility is for the unstable molecule to autoionize and eject an electron. This action puts the unstable molecule back into the bound molecular ion. The second possibility is for the unstable molecule to dissociate into two neutral atoms. This action is the completion of the dissociative-recombination reaction. Figure 3 shows the potential energy curves of the molecular ion and the unstable molecule crossing at the

point R_s . This point is called the stabilization point and is the internuclear separation distance that limits the time for autoionization. After the neutral atoms are separated by a distance greater than R_s , additional energy is necessary for the system of particles to return to the bound molecular ion state where autoionization can take place. Using the Born-Oppenheimer approximation, autoionization is impossible at internuclear separations greater than R_s . (Ref 12) The time necessary for autoionization is typically 10^{-14} sec, and the time necessary for the neutral atoms to separate to greater internuclear separation than R_s is 10^{-16} to 10^{-15} sec (Ref 12). Therefore, the dissociative recombination process is more likely to result in two neutral atoms than for the unstable molecule to autoionize.

The cross section for the dissociative recombination of a molecular ion into two neutral atoms is given in equation 55 where $\sigma(\epsilon)$ is the cross section for dissociative recombination as a function of incident electron energy ϵ , $\sigma_{cap}(\epsilon)$ is the cross section for the capture of an electron by the molecular ion to form the intermediate unstable molecule AB^{++} , and $S(\epsilon)$ is the probability that the intermediate unstable molecule survives long enough to dissociate and is called the survival factor (Ref 12).

$$\sigma(\epsilon) = \sigma_{cap}(\epsilon)S(\epsilon) \quad (55)$$

Previous arguments indicate that $S(\epsilon)$ is high for thermal electrons and can be considered approximately one.

The $\sigma_{\text{cap}}(\varepsilon)$ term is now examined. An assumption is made by Bardsley and Biondi that the unstable molecule AB^{**} is formed by the excitation of a target electron to create a higher excited state and the incident electron falls into an unoccupied orbital (Ref 12). Assuming $V(R)$ represents the electronic matrix element governing the configuration interaction, $\psi(r,R)$ represents the electronic wave functions of the molecules, $\zeta(R)$ represents the nuclear wave functions, $\phi_{\varepsilon}(r,R)$ represents the incident electron wave function, and r represents the ratio of multiplicities of the intermediate molecule AB^{**} to the initial molecular ion AB^{+} , $\sigma_{\text{cap}}(\varepsilon)$ is given in equation 56.

$$\sigma_{\text{cap}}(\varepsilon) = (2\pi^3/\hbar m \varepsilon) \left(\frac{r}{2}\right) |\langle \zeta_{AB^{+}}(R) | V(R) | \zeta_{AB^{**}}(R) \rangle|^2 \quad (56)$$

The ratio of multiplicities is divided by two to allow for the two possible spin orientations of the incident electron (Ref 12). The electronic matrix element $V(R)$ is given in equation 57 where $H_{\text{el}}(r,R)$ is the Hamiltonian for the molecular-electronic wave function.

$$V(R) = \langle \psi_{AB^{+}}(r,R) \phi_{\varepsilon}(r,R) | H_{\text{el}}(r,R) | \psi_{AB^{**}}(r,R) \rangle \quad (57)$$

The $(1/\varepsilon)$ proportionality for $\sigma_{\text{cap}}(\varepsilon)$ is developed in reference 13.

Figure 4 shows examples of the expected nuclear wave functions for AB^{+} and AB^{**} .

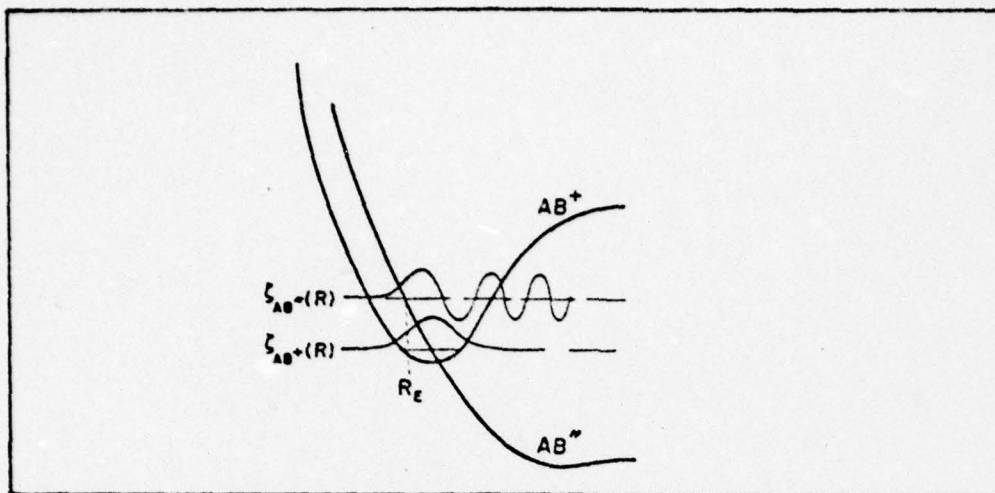


Fig. 4. Hypothetical potential energy curves and associated wave functions for one of the states of the molecular ion AB^+ and of the unstable molecule AB'' involved in the direct dissociative recombination process. (Ref 12)

The $\zeta_{AB''}(R)$ wave function shows a large probability of AB'' particle being near the classical turning point R_E . This wave function oscillates rapidly and decreases exponentially as the internuclear separation distance R grows greater than R_E . Bardsley and Biondi (Ref 12) approximate $\zeta_{AB''}(R)$ with a delta function located at R_c (Ref 19). By putting the delta function at R_c , Bardsley and Biondi require that R_c be close to R_E . The delta function is given in equation 58 where U' is the slope at R_c .

$$\zeta_{AB''}(R) = (1/U')^{1/2} \delta(R - R_c) \quad (58)$$

The requirement for the location of R_c is given in equation 59 where U indicates the potential energies of the molecules.

$$U_{AB^-}(R_c) - U_{AB^+}(R_c) = \epsilon \quad (59)$$

The ground-state nuclear wave function, $\zeta_{AB^+}(R)$ is approximated by a harmonic oscillator wave function. Substitution of these approximations into equation 56 yields equation 60.

$$\sigma_{\text{cap}}(\epsilon) = (2\pi^3/\hbar m \epsilon) \left(\frac{r}{2}\right) \left(\frac{1}{U}\right) |V(R_c)|^2 |\zeta_{AB^+}(R_c)|^2 \quad (60)$$

By defining the capture width Γ_c as $(\frac{2\pi}{\hbar})|V(R_c)|^2$, equation 60 reduces to equation 61.

$$\sigma_{\text{cap}}(\epsilon) = \left(\frac{\pi^2}{m \epsilon}\right) \left(\frac{r}{2}\right) \left(\frac{\Gamma_c}{U}\right) |\zeta_{AB^+}(R_c)|^2 \quad (61)$$

This development indicates that R_c must be within the range of nuclear vibrations so the probability of capture is greatest.

The reaction-rate constant for dissociative recombination is obtained by integrating over all energies for the product of the electron distribution, $f(\epsilon)$, the dissociative recombination cross section, $\sigma(\epsilon)$, and the electron velocity as in equation 62.

$$R_{\text{DR}} = \int_0^\infty \left(\frac{2\epsilon}{m}\right)^{1/2} \sigma(\epsilon) f(\epsilon) d\epsilon \quad (62)$$

If $f(\epsilon)$ is a Maxwell-Boltzmann distribution of electron energies, equation 62 reduces to equation 63 (Ref 12).

$$R_{DR} = (8/\pi m k^3 T_e^3)^{1/2} \int_0^{\infty} \sigma(\epsilon) \exp(-\epsilon/kT_e) \epsilon d\epsilon \quad (63)$$

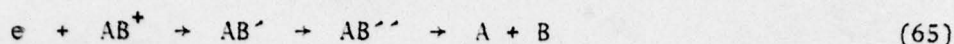
Bardsley and Biondi (Refs 12, 14, 15) present four assumptions that allow the dissociative recombination rate for the ground vibrational and electronic state to be expressed in terms of electron temperature T_e . These assumptions are:

- (i) The survival factor, $S(\epsilon)$, is almost one.
- (ii) The incident electron energy is less than 1 eV.
- (iii) U_{AB^+} is such that R_c is close to R_E .
- (iv) The vibrational wave function for AB^+ can be approximated by the ground state harmonic oscillator wave function.

The resultant dissociative-recombination reaction-rate constant is given in equation 64 where a is the amplitude of initial vibrational motion, R_0 is the equilibrium nuclear separation distance, and T_e is in units of $^{\circ}K$ (Ref 12).

$$R_{DR}(T_e) = 8.8 \frac{r_c^2}{U a} \exp\left(-\frac{(R_s - R_0)^2}{a^2}\right) \left(\frac{T_e}{500}\right)^{-0.5} \times 10^{-7} \text{ cm}^3 \text{ sec}^{-1} \quad (64)$$

Not all experimental data agree with $T_e^{-0.5}$ dependence in equation 64. This is the fact that led Bardsley (Ref 15) to investigate an alternate method of dissociative recombination. The alternate method is called indirect dissociative recombination and is represented in reaction 65.



The potential energy curves representing reaction 65 are given in Figure 5.

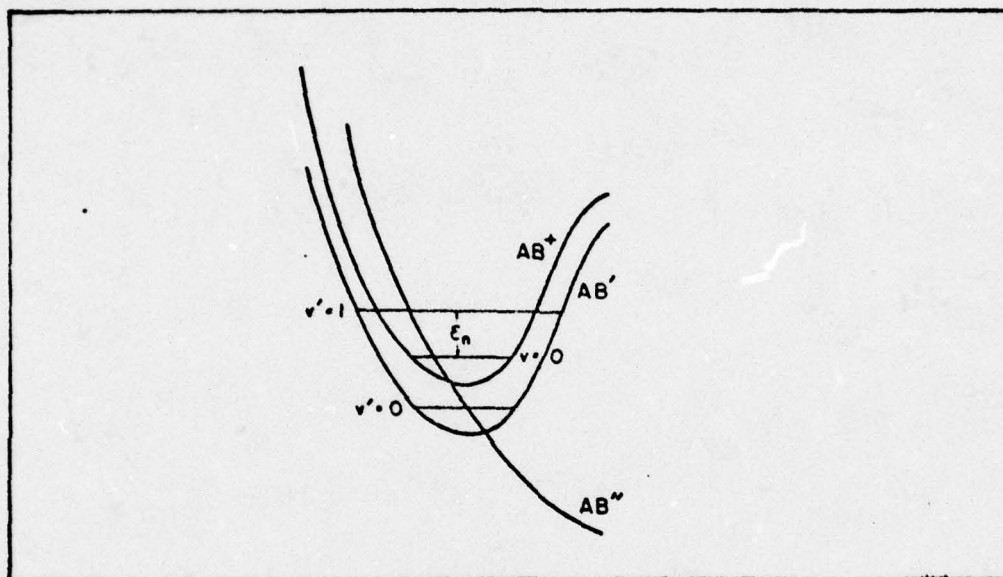


Fig. 5. Hypothetical potential energy curves for the molecular ion AB^+ , a highly stable Rydberg state AB' , and an unstable molecule curve AB'' involved in the indirect dissociative recombination process. The $v = 0$ vibrational level of the molecular ion AB^+ and the $v' = 0$ and 1 vibrational levels of the Rydberg state AB' are also shown (Ref 12).

In Figure 5, the energy contributed by the electron is ϵ_n . This energy must be close to the energy that is required to put the AB^+ state into a AB' Rydberg state. The electron energy is contributed to the nuclear motion of the AB' state. The excited Rydberg state predissociates to AB'' because of the location of the potential energy curve crossing, and normal dissociative recombination takes

place. The electron temperature dependence for the reaction-rate constant for reaction 65 is given in equation 66 where n is the possible number of Rydberg states.

$$R'_{DR}(T_e) = T_e^{-1.5} \sum_n c_n \exp(-\epsilon_n/kT_e) \quad (66)$$

The possibility exists for direct and indirect dissociative recombination for any given reaction. Therefore, the eventual theoretical temperature dependence can vary depending on the available Rydberg states and the electron temperature.

Experimental values and calculations. O'Mally et al. (Ref 16) find that, if the location of the stabilization point is shifted slightly, a better probability for dissociative recombination exists if the ionic molecule is in an excited vibrational state. The experimental data for neon is best fit by a low vibrational state model using parameters that are determined by a computer program (Ref 16). This model predicts the reaction-rate constant for neon to vary according to T_e and five set parameters.

Fortunately, experimental data for the dissociative recombination of Ar_2^+ and Xe_2^+ as a function of incident electron energy (Refs 17, 18) exists, and reasonable predictions for these reaction-rate constants can be made simply. Mehr and Biondi (Ref 17) find that the reaction-rate constant for Ar_2^+ varies as $T_e^{-0.67}$ for a gas temperature of 300° K. Assuming that the 0.03 eV increase in gas temperature of this model over Mehr and Biondi's (Ref 17) experiment does not affect the

vibrational distribution of the molecular ions greatly, Mehr and Biondi's $T_e^{-0.67}$ dependence is used to predict a dissociative-recombination reaction-rate constant of $3.9 \times 10^{-8} \text{ cm}^3/\text{sec}$ for Ar_2^+ in this model. Shiu et al. (Ref 18) find that for Xe_2^+ the dissociative-recombination reaction-rate constant varies as $T_e^{-0.72}$ for $T_e > 1000^\circ \text{ K}$ and a gas temperature of 300° K . Again, assuming the data that is reported for a gas temperature of 300° K are valid for the temperature of the model of 533° K , a dissociative-recombination reaction-rate constant of $8.16 \times 10^{-8} \text{ cm}^3/\text{sec}$ is calculated for Xe_2^+ .

Conclusion. The theory for dissociative recombination is difficult to use for predicting reaction-rate constants. Fortunately, sufficient experimental data exist and can be used to predict dissociative-recombination reaction-rate constants for higher electron energies. The data used for these predictions are for electron temperatures to 8000° K for Xe_2^+ and electron temperatures to 10000° K for Ar_2^+ (Refs 17, 18).

The assumption that data for gases at 300° K are valid for gases at 533° K is probably valid. The vibrational spacings of atmospheric diatomic ions are on the order of 0.2 eV (Ref 12). The energy difference between 300° K and 533° K is approximately 0.03 eV and probably is not near a vibrational level. Therefore, the reaction-rate constants for the dissociative recombination of Ar_2^+ and Xe_2^+ are at least close to the values that are predicted here.

The reaction-rate constant values of $3.9 \times 10^{-8} \text{ cm}^3/\text{sec}$ for Ar_2^+ and $8.16 \times 10^{-8} \text{ cm}^3/\text{sec}$ for Xe_2^+ are used in Chapter 4 for

calculations involving an applied electric field. With an applied electric field across the plasma, the average electron temperature is found to be approximately 4 eV (Ref 4). For electrons at these higher energies that are not in a Maxwell-Boltzmann distribution, it is best to measure the reaction-rate constant rather than the cross-section for the reaction.

For calculations in Chapter 4 that are made for no applied electric field, the electrons are assumed to be in thermal equilibrium with the gas. The dissociative-recombination reaction-rate constants that are used in this case are $5.99 \times 10^{-7} \text{ cm}^3/\text{sec}$ for Ar_2^+ and $1.88 \times 10^{-6} \text{ cm}^3/\text{sec}$ for Xe_2^+ . This assumption is discussed in Chapter 4.

The next section is about a similar process to dissociative recombination that is called dissociative attachment.

Dissociative Attachment

Introduction. Dissociative attachment, a process similar to dissociative recombination, involves the capture of an electron by a neutral molecule. The molecule then dissociates to form a negative atom and a neutral atom. The dissociative-attachment reaction in this model is reaction 9a shown below.



The theoretical description given in this section is only a general presentation that is based on Bardsley and Mandl (Ref 20) and the potential energy curves for Cl_2^- that are developed by Gilbert and

Wahl (Ref 21). The experimental data that is available for comparison to theory is primarily for dissociative attachment of Cl_2 by thermal electrons (Refs 11, 22, 23, 24).

Theoretical and experimental results. Dissociative attachment is the capture of electrons by neutral molecules and the dissociation of these now negative molecular ions each into a negative atom and a neutral atom. The one difference between dissociative recombination and dissociative attachment is the requirement that the neutral molecule involved in dissociative attachment must contain an atom with a high electron affinity. Electron affinity is the energy released when the neutral atom gains an electron. Gilbert and Wahl (Ref 21) find the electron affinity of ground state Cl_2^- to be 2.19 eV.

Bardsley and Mandl (Ref 20) describe dissociative attachment in a similar manner to dissociative recombination. The energy of the captured electron must be great enough to excite the target molecule to an energy greater than that of the potential energy of the intermediate molecular ion as is shown in Figure 6 (Ref 20). The experimental results of Frost and McDowell (Ref 25) provide some justification for this theoretical model. The experimental results give a threshold electron energy for the dissociative attachment of Cl_2 to be 1.6 eV and support the supposition that this dissociative attachment is the result of formation of $\text{Cl}_2^{-*} ({}^2\pi_g)$ state.

Recent experiments (Refs 11, 22, 23) for thermal energy electrons show that the threshold energy for the dissociative attachment of Cl_2 is not 1.6 eV. In fact, this experimental data shows that thermal electrons are attached to Cl_2 rapidly. Christodoulides et al. (Ref 11)

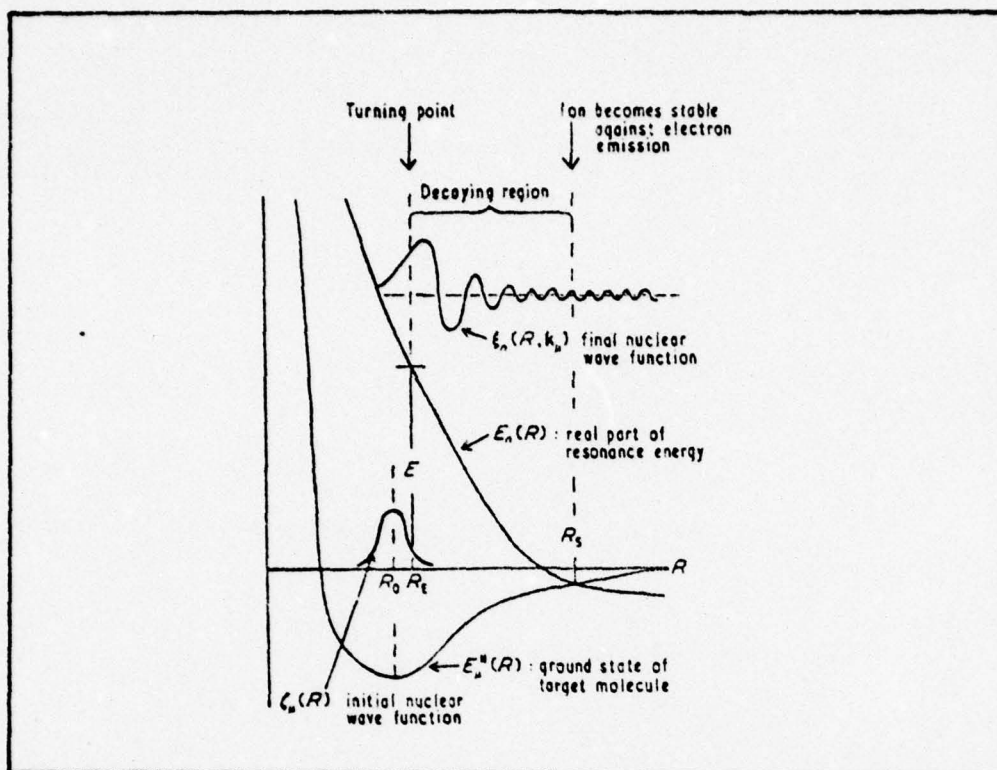


Fig. 6. Potential energy curves and nuclear wave functions in dissociative attachment. The final wave function is schematic only (Ref 20).

find the dissociative-attachment reaction-rate constant for Cl_2 to be $3.1 \times 10^{-10} \text{ cm}^3/\text{sec}$. Schultes et al. (Ref 22) report a broad maximum exists for the reaction-rate constant for dissociative attachment of Cl_2 between electron energies of 0.25 eV and 0.5 eV. Sides et al. (Ref 23) report a dissociative-attachment reaction-rate constant for Cl_2 of $(3.7 \pm 1.8) \times 10^{-9} \text{ cm}^3/\text{sec}$ for an electron temperature of 350° K . These experiments (Refs 11, 22, 23) confirm the formation of $\text{Cl}_2^- (^2\Sigma_u^+)$ for thermal electrons.

The potential energy curves that are presented by Gilbert and Wahl (Ref 21) are shown in Figure 7. These curves show the intersection of the Cl_2 potential energy curve by the $\text{Cl}_2^-(^2\Sigma_u^+)$ potential energy curve at the minimum of the Cl_2 potential well. The possible formation of $\text{Cl}_2^-(^2\Sigma_u^+)$ by thermal electron excitation from the Cl_2 potential curve to the $\text{Cl}_2^-(^2\Sigma_u^+)$ potential energy curve is apparent. The possibility of excitation from the Cl_2 potential energy curve to higher levels of Cl_2^- does exist.

Conclusion. The potential energy curves for Cl_2^- of Gilbert and Wahl (Ref 21) imply that a graph of the dissociative-attachment cross section for Cl_2 versus electron energy may contain several peaks corresponding to each excited potential energy curve of Cl_2^- . The location of these peaks depends on the electron energy required to excite the Cl_2 to Cl_2^- . Further research is required to determine the electron energy dependence of the dissociative-attachment reaction-rate constant for Cl_2 .

The reaction-rate constant for dissociative-attachment of Cl_2 by thermal electrons that is determined by Sides et al. (Ref 23), $3.7 \times 10^{-9} \text{ cm}^3/\text{sec}$, is used in this model.

The next section deals with the ion-neutral association reactions.

Ion-Neutral Association Reactions

Introduction. In this section two theories are discussed for atomic ion-neutral association. This reaction involves three atoms, one ionized and two neutral, as shown in reaction 67.

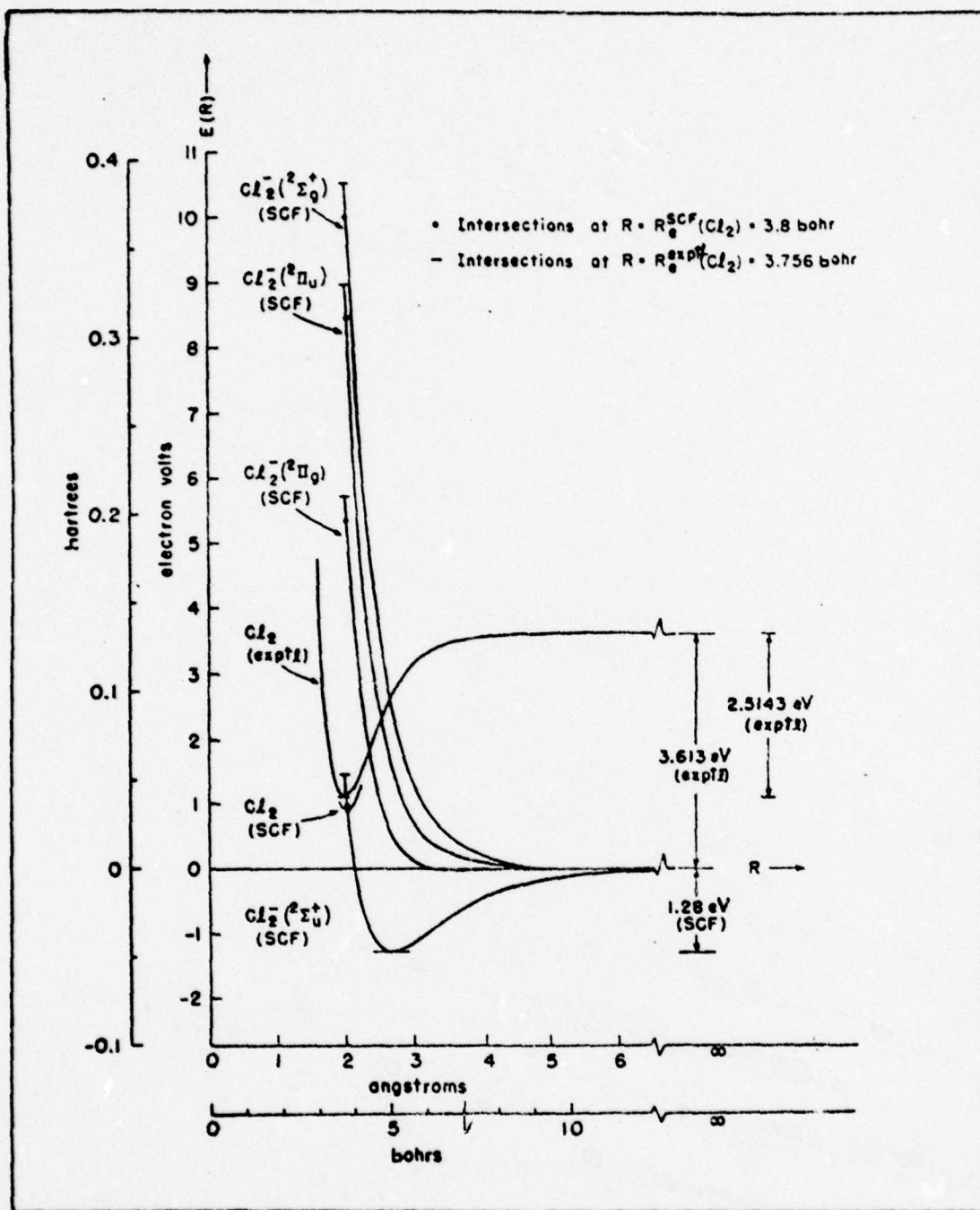
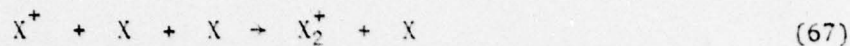


Fig. 7. Potential curves for Cl_2 and Cl_2^- (Ref 21)



Three reactions of this type are included in this model of the HgCl laser. These reactions involve the formation of Ar_2^+ and Xe_2^+ , and are steps in the charge-transfer process that creates Hg^+ . The first theory presented is Mahan's theory (Ref 26), and the second theory is Smirnov's theory (Ref 27).

Mahan's theory. Mahan's theory (Ref 26) is based on the assumption that the ion undergoes a resonant charge transfer with a second identical neutral particle while a third arbitrary particle is at some distance from the first two particles. In this charge transfer, a negligible amount of kinetic energy is lost. The second particle that is now charged is at some distance from a third arbitrary uncharged particle. If the relative kinetic energy of the third particle and the newly charged second particle is less than the negative potential energy of the two particles, a bound diatomic molecule is formed. Since no kinetic energy is transferred, this process is called a potential-energy transfer (Ref 26).

Mahan's next assumption is that the potential energy between the second and third particles is the ion-induced dipole type (Ref 26). Hirschfelder discusses the energy of ion-induced dipole type reaction in Reference 28. Mahan then assumes the ion-induced dipole potential does not affect the second and third particles until after the resonant charge transfer process takes place. This assumption means the charge transfer must take place in a short time. A fast charge

transfer occurs if the first and second particles are at a large separation distance (Ref 26), because the second particle spends less time in the sphere of interaction of particle 1 as the separation distance of the particles increases.

These assumptions lead to a bound-molecular ion being formed if the ion-induced dipole potential energy is greater than the neutral kinetic energy of the second and third particles. This condition is given in equation 68 where $(\frac{\alpha e^2}{2r^4})$ is the ion-induced dipole potential energy and $(\frac{1}{2} M_r v_r^2)$ is the relative kinetic energy of the second and third particles.

$$\frac{1}{2} M_r v_r^2 \leq \frac{\alpha e^2}{2r^4} \quad (68)$$

In equation 68, M_r is the reduced mass, v_r the relative speed, and r is the separation distance of the second and third particles. Also in equation 68, α is the polarizability of the third particle and e is the electron charge. Solving equation 68 for r shows that a bound molecule is not formed by the second and third particle unless equation 69 is true.

$$r_c = \left(\frac{\alpha e^2}{M_r v_r^2} \right)^{1/4} \quad (69)$$

The critical radius, r_c , is the maximum separation distance for the second and third particles to be apart and still form a bound molecule after the charge transfer takes place.

Mahan's reaction-rate constant for ion-neutral association is given by the product of the reaction-rate constant for charge transfer and the probability that the third particle is within a sphere of radius r_c that is centered at the second particle (Ref 26). This condition is shown in equation 70 where $f(v_r)$ is the relative speed distribution and R_{CT} is the reaction-rate constant for charge transfer of the first and second particles.

$$R_{I-N} = R_{CT} \frac{4\pi}{3} \int_0^{\infty} r_c^3(v_r) f(v_r) dv_r \quad (70)$$

Mahan states that the assumption of resonant charge transfer between the first and second particle is not strictly true if the third particle is close enough to the first and second particles to interfere with the charge transfer reaction. Mahan also states that for "typical values of ionization energy" this assumption is not incorrect enough to affect the results of his theory (Ref 26).

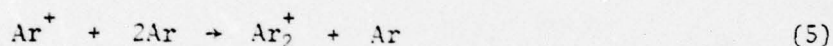
If the speed distribution of the reacting particle is assumed to be a Maxwell-Boltzmann distribution and equation 69 is substituted into equation 70, the reaction-rate constant for ion-neutral association is given by equation 71 and 71a (Ref 26).

$$R_{I-N} = R_{CT} \frac{16\pi^2}{3} \left(\frac{M_r}{2\pi kT}\right)^{3/2} \left(\frac{e^2}{M_r}\right)^{3/4} \int_0^{\infty} v_r^{1/2} \exp\left(-\frac{M_r v_r^2}{2kT}\right) dv_r \quad (71)$$

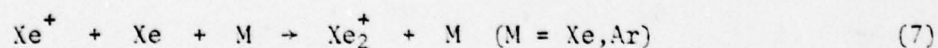
$$R_{I-N} = \frac{4}{3\pi} \frac{1}{2} \frac{1}{2} \Gamma(3/4) R_{CT} \left(\frac{\alpha e^2}{kT} \right)^{3/4} \quad (71a)$$

Mahan's calculated data is computed by multiplying the charge-transfer cross-sections of Dalgarno (Ref 29) by the root-mean-square relative speed. Mahan uses the polarizabilities of Pitzer (Ref 30) for the calculated values (Ref 26). Mahan's method of calculation appears to be reasonable, because his calculated values are all within a factor of three and most are within a factor of two of the experimental values (Ref 26).

Using Mahan's method of calculation and the data in references 29 and 30, a reaction-rate constant of $2.36 \times 10^{-31} \text{ cm}^6/\text{sec}$ is calculated for reaction 5 at 300° K .



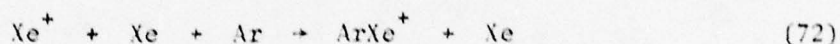
This value compares nicely to the experimental value obtained by Smith, Dean, and Plumb of $(2.50 \pm 0.10) \times 10^{-31} \text{ cm}^6/\text{sec}$ (Ref 31). The value that is calculated for reaction 5 at 533° K is $2.59 \times 10^{-31} \text{ cm}^6/\text{sec}$. The value that is calculated for reaction 7 at 300° K assuming M is Xe is $5.8 \times 10^{-31} \text{ cm}^6/\text{sec}$.



This value is within a factor of two of the experimental value of $(3.57 \pm 0.17) \times 10^{-31} \text{ cm}^6/\text{sec}$ that is reported by Smith, Dean, and Plumb (Ref 31), and it is within a factor of three of the value

$(2.0 \pm 0.2) \times 10^{-31}$ cm⁶/sec for reaction 7 reported by Vitols and Oskam (Ref 32).

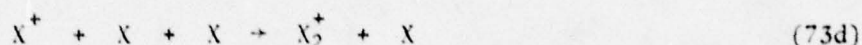
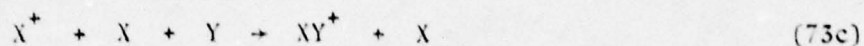
The reaction-rate constant for reaction 7 using Ar as a third body is not computable using Mahan's theory (Ref 26) and is an example of the limited applicability of Mahan's theory. This reaction-rate constant cannot be calculated, because Mahan's theory assumes charge transfer between the first and second particles and molecular formation between the second and third particle. If this method of formation is applied to reaction 7, this reaction is now reaction 72.



The products in reaction 72 can be formed in two ways. First, the charge transfer is between Xe^+ and Xe and the molecule ArXe^+ is formed. Second, the charge transfer is between Xe^+ and Ar and the molecule ArXe^+ is formed. The second method is not included in Mahan's theory, because Mahan requires charge transfer between identical particles.

Smirnov's theory. Smirnov's theory (Ref 27) is the solution to the problems presented by Mahan's theory. Smirnov's theory presents methods for the solution of reactions 73a, b, c, and d where X and Y are different atoms.





Smirnov first investigates reaction 73d.

Smirnov's theory is based on the assumption that the energy of the gas particles, which is proportional to the temperature of the gas, is much lower than the dissociation energy of a molecular ion (Ref 27). The rate of change of atomic ions into molecular ions is given in equation 74 where N_{MOL^+} is the molecular ion density, N_{AT^+} is the atomic ion density, N_A is the neutral atom density, and R_{I-N} is the reaction-rate constant for ion-neutral association.

$$\frac{dN_{MOL^+}}{dt} = R_{I-N} N_{AT^+} N_A^2 \quad (74)$$

Smirnov states that the potential energy of interaction between the atomic ion and neutral atom is determined by induced-dipole polarization interaction when the binding energy of the molecular ion is on the order of the gas temperature (Ref 27).

The $(R_{I-N} N_A^2)$ term from equation 74 is examined. This term is found to have the relationship shown in equation 75 (Ref 27).

$$R_{I-N} N_A^2 = N_A \langle \sigma v \rangle W \quad (75)$$

The $(N_A \langle \sigma v \rangle)$ term gives the frequency that a neutral atom creates

the potential to be bound with an atomic ion to form a molecular ion. The W term is the ratio of the probability that the molecular ion gives up energy in a collision with a third neutral atom and creates a more bound molecular ion to the probability that the molecular ion gains energy on the order of the temperature in a collision with third neutral atom and dissociates. As a result of the detailed balancing principle and for the induced-dipole polarization interaction, $W \sim (\frac{\alpha e^2}{T})^{3/4} N_A$ where α is the polarizability of the atom. Smirnov states that σ is proportional to $(\frac{\alpha e^2}{T})^{1/2}$ for the polarization interaction cross section for transition of the ion into weakly excited states (Ref 27). Equation 75 is now equation 76.

$$R_{I-N} N_A^2 \sim N_A \langle v \rangle (\frac{\alpha e^2}{T})^{1/2} (\frac{\alpha e^2}{T})^{3/4} N_A \quad (76)$$

Because the velocity is proportional to $(\frac{T}{M})^{1/2}$ for a Maxwell-Boltzmann distribution, equation 76 transforms to equation 77 where M is the mass of the gas atoms.

$$R_{I-N} = \text{constant} (\frac{\alpha e^2}{M})^{1/2} (\frac{\alpha e^2}{T})^{3/4} \quad (77)$$

Equation 77 is true for reaction 7d.

Smirnov forces equation 77 to equate to 1.1×10^{-31} cm⁶/sec for reaction 73d where X is He and the temperature is 300° K. This process results in a value for the constant of approximately 42 in equation 77 (Ref 27).

The results using Smirnov's theory (Ref 27) are not as good as those using Mahan's theory (Ref 26). Using the data from Pitzer (Ref 30), a reaction-rate constant of 5.24×10^{-31} cm⁶/sec is calculated for Ar ion-neutral association in reaction 5 at a temperature of 300° K. This value is more than a factor of two greater than both the value of 2.36×10^{-31} cm⁶/sec from Mahan's theory and the experimental value of $(2.5 \pm 0.10) \times 10^{-31}$ cm⁶/sec (Ref 31) at the same 300° K temperature. The value that is calculated for reaction 7 at 300° K with Xe as the third body using Smirnov's theory is 8.88×10^{-31} cm⁶/sec. This value is more than a factor of two greater than the experimental value of $(3.57 \pm 0.17) \times 10^{-31}$ cm⁶/sec (Ref 31). Mahan's theory gives a value within a factor of two of the experimental value. Smirnov's theory does give results within a factor of three of the experimental results for reactions 5 and 7.

Smirnov (Ref 27) modifies equation 77 using Thomson's theory (Ref 33) to give reaction-rate constants valid for reaction 73a, b, and c. The assumption necessary for this modification is that the mass, m , of particle Y is less than the mass, M , of particle X. The reaction-rate constants for reactions 73a, b, and c are given in equations 77a, b, and c, respectively (Ref 27).

$$R_{I-N} = 42 \left(\frac{m}{M}\right)^{1/4} \left(\frac{\alpha_Y e^2}{T}\right)^{3/4} \left(\frac{\alpha_Y e^2}{m}\right)^{1/2} \quad (77a)$$

$$R_{I-N} = 42 \left(\frac{m}{M}\right)^{1/4} \left(\frac{\alpha_X e^2}{T}\right)^{3/4} \left(\frac{\alpha_Y e^2}{m}\right)^{1/2} \quad (77b)$$

$$R_{I-N} = 42 \left(\frac{\alpha_Y e^2}{T} \right)^{3/4} \left(\frac{\alpha_X e^2}{M} \right)^{1/2} \quad (77c)$$

Smirnov (Ref 27) notes the value, 1.5×10^{-31} cm⁶/sec, that is calculated for reaction 78 at approximately 400° C is close to Biondi's experimental value (Ref 34) of 1.7×10^{-31} cm⁶/sec.



This close agreement for one reaction does not imply that a greater accuracy than the factor of three that is applied to equation 77 is applied to equations 77a, b, and c.

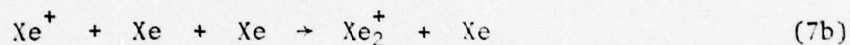
The value that is calculated for reaction 7 using Ar as a third body and Smirnov's equation 77b is 4.96×10^{-31} cm⁶/sec at 533° K. The value that is calculated for reaction 7 using Xe as a third body and Smirnov's equation 77 is 5.77×10^{-31} cm⁶/sec at 533° K. Reaction 7a is reaction 7 with Ar as the third body, and reaction 7b is reaction 7 with Xe as the third body.



Conclusion. Mahan's theory (Ref 26) appears to predict reaction-rate constants to within a factor of two of known experimental results. This theory is limited in applicability, because Mahan requires a

specific order of charge transfer and interaction. Smirnov's theory (Ref 27) applies to more types of reactions than Mahan's theory. The values predicted by Smirnov's theory are probably within a factor of three of known experimental values. Therefore, Mahan's theory gives more accurate results for a limited number of reactions, and Smirnov's theory gives results for some types of ion-neutral association reactions not computable from Mahan's theory.

The following values are used in the model for ion-neutral reaction-rate constants. The experimental value (Ref 31) of $2.5 \times 10^{-31} \text{ cm}^6/\text{sec}$ is used in the model for reaction 5. The experimental value (Ref 31) of $3.6 \times 10^{-31} \text{ cm}^6/\text{sec}$ is used for reaction 7b. Reaction 7b is reaction 7 with Xe as the third body.



The value that is calculated using Smirnov's equation 77a, $4.96 \times 10^{-31} \text{ cm}^6/\text{sec}$, is used for reaction 7a. Reaction 7a is reaction 7 with Ar as the third body.



The next section is a summary of the charge transfer reactions in this model.

Charge Transfer Reactions

Introduction. The charge transfer processes that are included in this section are the near-symmetric charge transfers in reactions 6 and 8 of this model. The energy of the particles is approximately 0.07 eV. The charge transfer between Xe_2^+ and Hg in reaction 8 is a near-symmetric charge transfer (Ref 35). The general form of reactions to be considered in this section is shown in equation 79 where X is an atom and Y is a different atom.



Two theories are presented. The first theory is that of Gioumousis and Stevenson (Ref 36). The values generated by using Gioumousis and Stevenson's theory are in excellent agreement with the experimental values reported by Bohme et al. (Ref 37). The second theory is a brief presentation of Rapp and Francis' theory for the low-velocity region (Ref 38). The particles in reactions 6 and 8 are in the Rapp and Francis low-velocity region that is determined by the approximate upper limit $v \approx (10^5/M_r^{1/2})$ cm/sec where M_r is the reduced mass of the reacting particles in amu. Since the velocity of the gas particles is proportional to the square roots of the temperature of the gas, the Rapp-Francis low velocity region is defined by the gas temperature and the reduced mass of the reacting particles.

Gioumousis and Stevenson's theory. Gioumousis and Stevenson's theory is based on the fact that the long-range potential between an

ion and a neutral particle is given by equation 80 which is the ion-induced dipole polarization potential (Ref 36).

$$U = - \frac{e^2 \alpha_B}{2r^4} \quad (80)$$

In equation 80, U is the potential energy, e is the electronic charge, α_B is the polarizability of the neutral particle, and r is the separation distance of the ion and the neutral particle. Gioumousis and Stevenson use Langevin's (Ref 39) equation below describing the orbits for the ion-induced dipole potential (Ref 36). Equation 81 describes these orbits where b_0 is the impact parameter.

$$b_0 = \left(\frac{4e^2 \alpha_B}{M_r v_r^2} \right)^{1/4} \quad (81)$$

In equation 81, M_r is the reduced mass of the reacting particles and v_r is their relative velocity. A typical set of trajectories is included in Figure 8. The important facts in Figure 8 are that for $b < b_0$ the orbits pass through the center point and for $b \geq b_0$ the orbiting particles are never closer than $(b_0/\sqrt{2})$.

The next step in the development of this theory is the supposition that a critical radius, r_c , for a given reaction to take place exists (Ref 36). This critical radius is such that the probability of the reaction taking place is zero if the particle passes outside the critical radius and one if the particle passes inside the critical radius. Therefore, if $r_c \leq b_0/\sqrt{2}$ the cross section of interaction is given in equation 82.

$$\sigma = \pi b_0^2 = \pi \left(\frac{4e^2 \alpha_B}{M_r v_r^2} \right)^{1/2} \quad (82)$$

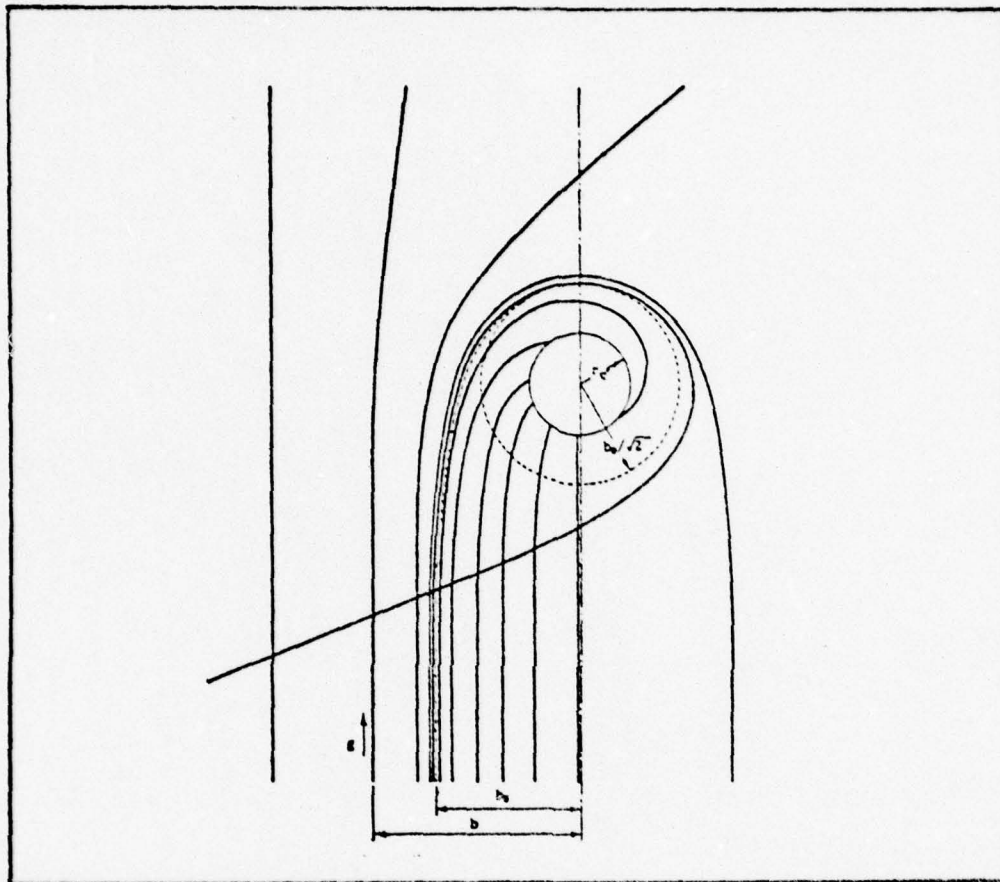


Fig. 8. A typical family of trajectories as a function of the impact parameter b . The dotted trajectory is the critical one for $b = b_0$ and approaches the circle $r = b_0 / \sqrt{2}$. Only trajectories with $b < b_0$ will enter the reaction sphere if it has radius r_c less than this, i.e., $r_c < b_0 / \sqrt{2}$. Thus, the cross section for entrance into the reaction sphere depends on b_0 but not, within limits, r_c . On the assumption that all molecules which enter the reaction sphere do react, the same may be said of the interaction cross section (Ref 36).

The larger cross sections are given for interactions between particles that maximize b_0 . This maximization is done by particles with a large polarizability, small reduced mass, and small velocities.

Since velocities are often described in terms of a velocity distribution, some higher velocities are certain to exist so that the condition $r_c < b_0/\sqrt{2}$ is not true. If the number of particles exceeding this criteria is kept to a minimum, this theory is still relatively valid (Ref 36).

The cross section in equation 82 multiplied by the relative velocity of the two particles is a constant shown in equation 83.

$$v_r \pi \left(\frac{4e^2\alpha_B}{M_r v_r^2} \right)^{1/2} = 2 \pi \left(\frac{e^2\alpha_B}{M_r} \right)^{1/2} = R_{CT} \quad (83)$$

Therefore, the expectation value of $\langle v_r \sigma(v_r) \rangle$ is the constant given in equation 83 for ions and neutral particles in a Maxwell-Boltzmann distribution. This constant is the reaction-rate constant for symmetric charge transfer.

Rapp and Francis' theory. The Rapp and Francis theory (Ref 38) for the low-velocity region, $v \leq \left(\frac{10^5}{M_r} \right)^{1/2}$, is a modification of the Gioumouis and Stevenson theory (Ref 36). Rapp and Francis say that the charge exchange probability is 0.5 for symmetric-charge-transfer reaction resulting from impact collisions (Ref 38). By multiplying this factor of 0.5 times the Gioumouis and Stevenson cross section of reaction given in equation 82, Rapp and Francis give a lower bound cross section for symmetric charge transfer shown in equation 84.

$$\sigma_{\text{lower}} = \frac{\pi e}{v_r} \left(\frac{\alpha_B}{M_r} \right)^{1/2} \quad (84)$$

Using the approximate value of 10^{-24} cm^3 for the polarizability of particle B allows Rapp and Francis to approximate the cross section. This approximate cross section is given in equation 85 where M_r is in amu and v_r is in cm/sec.

$$\sigma_{\text{lower}} \approx 1.2 \times 10^{-9} / (M_r^{1/2} v_r) \text{ cm}^2 \quad (85)$$

Experimental data. The charge-transfer experiments of Bohme et al. (Ref 37) provide excellent results for comparison to the theoretical reaction-rate constants that are calculated using Gioumouis and Stevenson's theory (Ref 36). For example, the theoretical value for reaction 86 is $5.73 \times 10^{-10} \text{ cm}^3/\text{sec}$ at 200° K , and the experimental value is $7.5 \times 10^{-10} \text{ cm}^3/\text{sec}$ (Ref 37).



Most of Bohme's data (Ref 37) is within a factor of two of the theoretical values. The values not within a factor of two of the theoretical values are less than the theoretical values and are best explained as reactions that are dominated by asymmetric charge transfers (Ref 37). The experimental data of Maier for particles with greater than thermal energies does not agree with Bohme's data (Ref 40). Therefore, Gioumouis and Stevenson's theory can be used for calculating theoretical values of charge-transfer reaction-rate constants for particles with thermal energies. These theoretical values can be considered to be within a factor of two of the upperlimit reaction-rate constants. If the charge transfer is asymmetrical, the

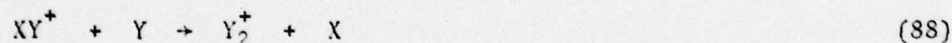
theoretical value places an upper limit on the reaction-rate constant.

The theoretical value for reaction 6 in this model, Ar_2^+ transferring charge to Xe, is $6.65 \times 10^{-10} \text{ cm}^3/\text{sec}$. The theoretical value for reaction 8 in this model, Xe_2^+ transferring charge to Hg, is $3.11 \times 10^{-10} \text{ cm}^3/\text{sec}$. The polarizability of Xe from Pitzer (Ref 30) is used in the calculation for reaction 6. An estimated value of $2 \times 10^{-24} \text{ cm}^3$ is used for the polarizability of Hg in reaction 8.

Bohme et al. (Ref 37) also use Gioumousis and Stevenson's theory (Ref 36) to calculate theoretical values for reactions similar to reaction 87.



The general form of reaction 87 is shown in reaction 88 where X and Y are different atoms.



This theoretical value for reaction 87 is $5.21 \times 10^{-10} \text{ cm}^3/\text{sec}$, and the experimental reaction-rate constant is $3.2 \times 10^{-10} \text{ cm}^3/\text{sec}$ (Ref 37). The theoretical values that are calculated for this type reaction are generally high by a factor of three or less (Ref 37).

Conclusion. The Gioumousis and Stevenson theory (Ref 36) results in reaction-rate constants within a factor of two for reactions similar to reaction 79 for particles with thermal energies. If the reaction is an asymmetric charge transfer, the theoretical value is an upper-limit reaction-rate constant. The Rapp-Francis theory (Ref 38) at low-velocities is not as accurate as the Gioumousis and Stevenson theory. The Rapp-Francis criteria for determining low-velocity reactions is probably a reasonable criteria for determining the applicability of the Gioumousis and Stevenson theory. The fact that the Gioumousis and Stevenson theory does not predict accurate reaction-rate constants for energies greater than thermal energies is pointed out in a comparison of Bohme's thermal energy data (Ref 37) to Maier's data (Ref 40) for energies greater than thermal. Therefore, the Gioumousis and Stevenson theory gives excellent reaction-rate constants for the charge-transfer reactions that are similar to reactions 6 and 8 with thermal energy reactants.

The next section includes discussion about the three ionic recombination processes in this model.

Ion-Ion Recombination

Introduction. Ion-ion recombination reaction is the process by which a singly ionized ion combines with a negative ion that has one extra electron. The four theories investigated in this section are J. J. Thomson's theory (Ref 33), Langevin's theory (Ref 41), Natanson's theory (Ref 41), and Wadehra and Bardsley's theory (Ref 42).

Thomson's theory. Thomson's theory of ionic recombination (Ref 33) is based on two assumptions. First, all gases are in thermal equilibrium. Second, if two oppositely charged ions pass within a certain distance of each other, called the trapping radius, these ions recombine (Ref 43). This development is similar to that in Reference 43.

The assumption that all ions are in thermal equilibrium with the gas means the average kinetic energy of the ions is equal to the average energy of any particle in the gas. This relationship is shown in equation 89 where m^{\pm} are the ionic masses, v_R^{\pm} are the root mean square velocities of the ions, T is the temperature of the gas in $^{\circ}\text{K}$, and k is the Boltzmann constant.

$$\frac{1}{2} m^{+} v_R^{+2} = \frac{1}{2} m^{-} v_R^{-2} = \frac{3}{2} kT \quad (89)$$

If the distance between the oppositely charged ions is large, then equation 90 is true where M_r is the reduced mass of m^{-} and m^{+} , and v_{OR} is the root-mean-square velocity of the relative velocities of the ions.

$$\frac{1}{2} M_r v_{OR}^2 = \frac{3}{2} kT \quad (90)$$

The next assumption is that the potential energy between the two ions is only Coulombic. This assumption means that as the ions are separated by greater and greater distances, the Coulomb potential energy, $-e^2/r$, approaches zero.

Thomson's assumption that leads to the idea of a trapping radius is that two ions recombine if their potential energy and kinetic energy sum to a negative number. Equation 90 shows the average kinetic energy of the two-ion system is $\frac{3}{2} kT$, which is positive. Since the two ions gain kinetic energy equal to their loss of potential energy as the two ions approach each other, the only way the kinetic energy is ever less than the magnitude of the potential energy is for kinetic energy to be given up in a collision with a third body. The kinetic energy of the ion starts at $\frac{3}{2} kT$ and increases as it approaches the other ion. If an ion is returned to an equilibrium temperature by a collision, then that ion is trapped when $e^2/r \geq \frac{3}{2} kT$. The distance, r_T , at which this occurs is called the trapping radius.

$$r_T = \frac{2e^2}{3kT} \quad (91)$$

Thomson's next assumption is that each ion is surrounded by a sphere with a radius equal to the trapping radius. The number of positive ions entering a sphere of interaction around a negative ion with radius r_T is $\pi r_T^2 n_+ (v_m^{+2} + v_m^{-2})^{1/2}$, where πr_T^2 is the circle of interaction, n_+ is the number density of positive ions, and $(v_m^{+2} + v_m^{-2})^{1/2}$ is the average relative velocity of the ions. The number of negative ions entering a positive sphere is $\pi r_T^2 n_- (v_m^{+2} + v_m^{-2})^{1/2}$, where n_- is the number density of negative ions. Let w^\pm be the probabilities that a positive or negative ion entering an appropriate sphere of interaction collides with another

particle and is thermalized in that sphere. The number of recombinations per cubic centimeter per second is then given in equation 92.

$$\dot{n}_{\text{recombinations}} = \pi r_T^2 n_+ n_- (v_m^{+2} + v_m^{-2})^{1/2} (w^+ + w^-) \quad (92)$$

An approximate value for w^\pm can be calculated using classical mechanics and ignoring the charges of the two ions. First, the probability that a particle travels a distance x in a gas and does not collide with another particle is $e^{-x/\lambda}$, where λ is the mean free path of the moving particle. The mean free path is a function of the total gas density and is not a function of only n_+ and n_- . Second, the distance x traveled by a particle in the sphere is given by equation 93.

$$x = 2r_T \cos \theta \quad (93)$$

The angle θ is formed by the intersection of the trajectory line and the line formed by the point of entry to the circle and the center of the circle. Third, the probability that a particle enters the circle of interaction between θ and $\theta+d\theta$ is $\sin \theta$ (Ref 44). Therefore, the probability that a particle enters a circle with radius r_T and collides with another particle is given in equation 94.

$$\begin{aligned} \left\{ \begin{array}{l} \text{Probability of} \\ \text{Collision} \end{array} \right\} &= 1 - \int_0^{\pi/2} e^{-2r_T \cos \theta / \lambda} \sin \theta d\theta \\ &= 1 - \frac{\lambda}{2r_T} (1 - e^{-2r_T/\lambda}) \end{aligned} \quad (94)$$

The actual probabilities of collision are greater than those calculated in equation 94, because the effect of the difference in charge is ignored.

Substituting w^\pm in equation 92 and dividing by $(n_+ n_-)$ results in the reaction-rate constant for ion-ion recombination given in equation 95 where λ_\pm are the mean free paths of the positive and negative ions.

$$R_{I-IR} = \pi r_T^2 (v_m^{+2} + v_m^{-2})^{1/2} \left[1 - \frac{\lambda_+}{2r_T} (1 - e^{-2r_T/\lambda_+}) + 1 - \frac{\lambda_-}{2r_T} (1 - e^{-2r_T/\lambda_-}) \right] \quad (95)$$

If the ions and the gas are assumed to be in a Maxwell-Boltzmann distribution, $(v_m^{+2} + v_m^{-2})^{1/2}$ equals $(\frac{8kT}{\pi M_r})^{1/2}$.

Two cases can be derived for equation 95. The first case is for low pressure gases. At low pressures, λ_\pm are large and e^{-2r_T/λ_\pm} can be estimated by the first three terms of the series representation for e^{-y} where y is small. The term w^+ is approximately r_T/λ_+ , and w^- is approximately r_T/λ_- . The reaction-rate constant for low pressure ion-ion recombination is given in equation 96.

$$R_{low} = 2\pi r_T^3 \left(\frac{8kT}{\pi M_r}\right)^{1/2} \left(\frac{1}{\lambda_+} + \frac{1}{\lambda_-}\right) \quad (96)$$

The second case is for high pressure gases. At high pressures, λ_\pm are small and e^{-2r_T/λ_\pm} approaches one. The reaction-rate constant for high pressure is given in equation 97.

$$R_{\text{high}} = 2\pi r_T^2 \left(\frac{8kT}{\pi M_r}\right)^{1/2} \quad (97)$$

Substituting equation 91 into equations 96 and 97 results in equations 96a and 97a.

$$R_{\text{low}} = \frac{32}{27} \left(\frac{2\pi}{M_r}\right)^{1/2} \frac{e^6}{(kT)^{5/2}} \left(\frac{1}{\lambda_+} + \frac{1}{\lambda_-}\right) \quad (96a)$$

$$R_{\text{high}} = \frac{16}{9} \left(\frac{2\pi}{M_r}\right)^{1/2} \frac{e^4}{(kT)^{3/2}} \quad (97a)$$

Equations 96a and 97a contain some interesting information.

The low pressure equation 96a indicates that at a constant temperature the reaction-rate constant increases with pressure. The high pressure equation 97a shows that the ion-ion recombination reaction-rate constant is independent of pressure at constant temperature.

Several other comments are made in Reference 43 concerning the low pressure equation 97a, the main point being that the Thomson low pressure reaction-rate constant for ion-ion recombination is a good approximation for pressures less than 1 atmosphere.

The fact that the Thomson high pressure reaction-rate constant is independent of pressure is in disagreement with experimental data (Ref 45). The reason for Thomson's generally high prediction of the recombination constant is that no consideration is given to the possibility of multiple collisions inside the sphere of interaction knocking a possible reacting particle out of the sphere of interaction.

Also, no consideration is given to dissociative collisions between molecules (Ref 46). These facts cause the Thomson theory generally to overestimate the high pressure reaction-rate constant for ion-ion recombination.

Langevin's theory. Langevin's theory is valid only at very high pressures and is based on the assumption that the attractive forces between two neighboring particles is Coulombic. The positive and negative ions drift toward each other at a rate determined by their mobilities K^{\pm} . The relative drift velocity, v_D , at a separation distance r of the two ions is $(K^+ + K^-) e^2/r^2$, where the effective electric field on the two ions is e^2/r^2 . If each negative particle is enclosed in a sphere of radius r , the number of positive particles entering the sphere is given by the product of the drift velocity, the surface area of the sphere, and the number density of negative ions. The number of recombinations is shown in equation 98.

$$\dot{n}_{\text{recombinations}} = 4\pi e^2 (K^+ + K^-) n^+ n^- \quad (98)$$

Langevin's reaction-rate constant for ion-ion recombination is given in equation 99.

$$R_{I-IL} = 4\pi e^2 (K^+ + K^-) \quad (99)$$

Langevin's theory does agree with Machler's data at 5 to 12 atmospheres of pressure (Ref 41). Langevin's theory also predicts a decrease in the reaction-rate constant as pressure increases.

The major problem that is found for using Langevin's theory for quick calculations for ion-ion recombination is the lack of data for K^\pm .

Natanson's theory. Natanson's theory (Ref 47) fills the gap between high and low pressures. Unfortunately, Natanson's theory requires more data than either Thomson or Langevin to calculate the reaction-rate constant for ion-ion recombination. The requirement by both Langevin and Natanson for data that is difficult to obtain in calculating the reaction-rate constants, forces the use of Thomson's theory for approximate calculations of ion-ion recombination reaction-rate constants.

Wadehra and Bardsley's theory. Wadehra and Bardsley's theory (Ref 42) is an extension of Natanson's theory to allow the masses and collision properties of the positive and negative ions to be different. By allowing for different collision properties for the positive and negative ions, a trapping radius is developed for the positive ion that is different from the trapping radius of the negative ion. Wadehra and Bardsley cite several sources of data for their calculations.

Conclusion. The use of Thomson's theory may not prove to be as inaccurate as expected in the calculations for ion-ion recombination in the HgCl laser. First, the ion-ion recombinations in the HgCl laser are atom-atom recombinations and not molecule-molecule recombinations. This fact eliminates the problem of dissociative collisions considered by Brueckner (Ref 46). Second, the operating pressure for the HgCl laser being investigated in this model is approximately 3.17 atmospheres. This pressure is not the extremely

high pressure at which Langevin's theory is accurate. This pressure is probably such that the reaction-rate constant is closer to its maximum value. Evidence of this fact is given in a theoretical calculation done by M. R. Flannery. Flannery's calculations for Hg^+ and Cl^- ionic recombination result in a maximum recombination constant of $2.4 \times 10^{-6} \text{ cm}^3/\text{sec}$ at N/N_L of 1.6. This reaction-rate constant drops rapidly to $1 \times 10^{-6} \text{ cm}^3/\text{sec}$ at $N/N_L = 9.0$ (Refs 48, 49). In the term N/N_L , N is the density of the third body Ar, and N_L is Loschmidt's number that is adjusted for temperature. If the assumption is made that the sum of the number densities of Xe and Ar in this model is a good approximation for N , an ionic recombination reaction-rate constant of $2.15 \times 10^{-6} \text{ cm}^3/\text{sec}$ is found from Flannery's data to apply to this model. Flannery's data is included in Appendix C.

Wadehra and Bardsley (Ref 42) predict an ionic recombination rate of $2.3 \times 10^{-6} \text{ cm}^3/\text{sec}$ for Ar^+ and Cl^- . This rate is computed for a gas temperature of 300° K and a pressure of approximately 3.1 atmospheres. The predicted ionic recombination rate for Hg^+ and Cl^- at the same temperature and pressure is $1.8 \times 10^{-6} \text{ cm}^3/\text{sec}$.

Three ion-ion recombination reaction-rate constants based on Thomson's theory are used in this model of the HgCl laser. These values result from calculations using equation 97a and are presented in Table 1.

Table 1
Ion-Ion Recombination Constants for the HgCl Laser

<u>Reaction</u>	<u>Reaction-Rate Constants</u> <u>(cm³/sec)</u>
$\text{Ar}^+ + \text{Cl}^- \rightarrow \text{ArCl}^*$	2.13×10^{-6}
$\text{Xe}^+ + \text{Cl}^- \rightarrow \text{XeCl}^*$	1.75×10^{-6}
$\text{Hg}^+ + \text{Cl}^- \rightarrow \text{HgCl}^*$	1.685×10^{-6}

These approximate values calculated for the HgCl laser are probably within a factor of three of the actual values. This hypothesis of close agreement is based on the excellent agreement of the value calculated using Thomson's model with Flannery's Hg^+ and Cl^- ionic recombination (Ref 48) at similar operating pressures. Wadehra and Bardsley's calculations (Ref 42) also provide excellent data and agreement with values calculated using Thomson's theory.

The next section includes a discussion of the harpooning theory as it is applied to this model.

Harpooning and Similar Reactions

Introduction. The harpooning reaction shown in reaction 100 usually involves an alkali atom, M, harpooning a diatomic halogen molecule, X_2 .



The theory that is presented in this section is based on Herschbach's (Ref 50) review of the harpooning reaction. The experimental data

(Ref 6) that is included in this section shows that excited states of some atoms are similar to alkali atoms and that these excited states are involved in reactions similar to harpooning reactions. Reactions such as Ar^* and Xe^* reacting with Cl_2 to form ArCl^* and XeCl^* are also included in this section.

Theory. The basic assumption that is made by Magee (Ref 51) is that the potential energy curves of MX and $(\text{M} + \text{X})$ cross at some point r_c that is called the capture point. This crossing is shown in Figure 9 for KBr (Ref 50). At the internuclear separation distance r_c , the Coulombic attraction forces are dominant. The capture point, r_c , can be determined by finding the energy that is required to form the ion pair. The energy that is required for this reaction is essentially determined by the amount of energy that is required to strip an electron from the alkali atom minus the energy that is given up by the halogen atom after the halogen atom captures the electron of the alkali atom. Equation 101 (Ref 50) shows the potential energy equal to the energy that is required for the harpoon reaction.

$$e^2/r_c = I(\text{M}) - E(\text{X}) \quad (101)$$

In equation 101, e is the electronic charge, $I(\text{M})$ is the ionization potential of the alkali atom, and $E(\text{X})$ is the electron affinity of the halogen atom.

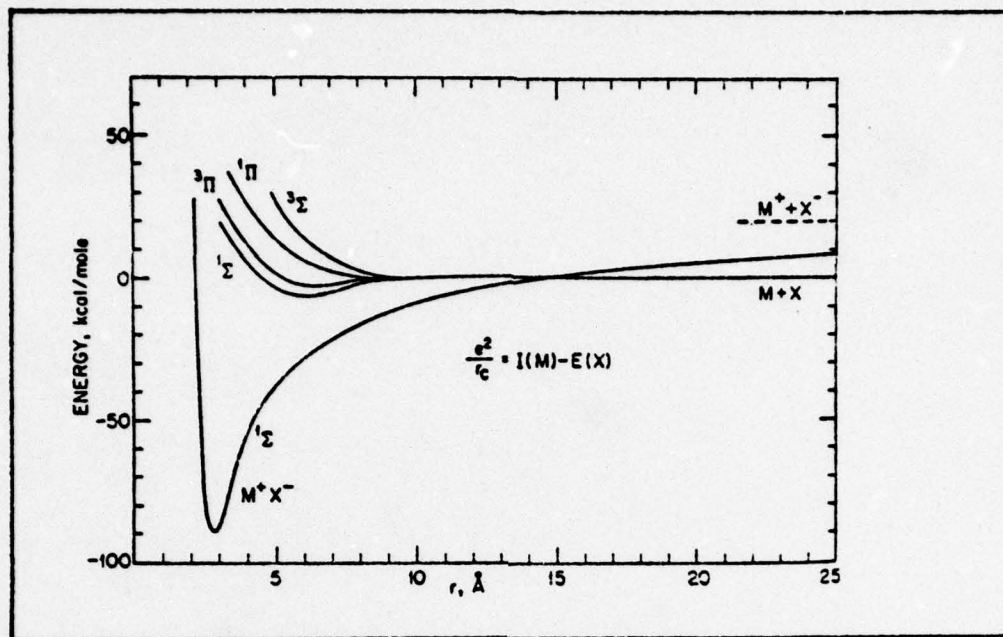


Fig. 9. Potential energy curves for an alkali halide molecule (drawn for KBr) showing the "zeroth-order crossing" of the ionic and covalent states (Ref 50).

Krause et al. (Ref 6) hypothesize that the $\text{Hg}^* ({}^3\text{P}_2)$ reaction with Cl_2 to form HgCl^* is similar to the harpoon reaction. A calculation using an ionization potential of 4.974 eV (Ref 6) for $\text{Hg}^* ({}^3\text{P}_2)$ and an electron affinity of 2.19 eV for Cl_2 (Ref 21) results in a reaction cross section of 84.3 \AA^2 . This cross section is calculated by using πr_c^2 as the reaction cross section. This calculated cross section is in good agreement with the experimental cross section for this reaction that is determined by Kraus et al. of $(90 \pm 25) \text{ \AA}^2$ (Ref 6).

Experimental work. By multiplying the experimental cross section of Kraus et al. (Ref 6) by the average relative velocity of the Hg^* and Cl_2 in this model, a reaction-rate constant of $4.18 \times 10^{-10} \text{ cm}^3/\text{sec}$

is calculated for HgCl^* formation by Hg^* harpooning of Cl_2 . These gas particles in the model are assumed to be in a Maxwell-Boltzmann distribution at a temperature of 533°K .

Reactions that are included in this model that are similar to the HgCl^* formation by Hg^* and Cl_2 are the formation of ArCl^* by Ar^* and Cl_2 and the formation of XeCl^* by Xe^* and Cl_2 . The reaction-rate constants for these reactions are calculated assuming these gas particles are in a Maxwell-Boltzmann distribution at 533°K . The XeCl^* formation reaction-rate constant is calculated using the quenching cross section for Xe^* by Cl_2 that is reported by Velazco and Setser to be 210 \AA^2 (Ref 52). Velazco and Setser (Refs 52, 53) report that almost 100% of the quenching of Xe^* by Cl_2 includes the formation of XeCl^* . Therefore, the total quenching cross section is multiplied by the average relative velocity to get a reaction-rate constant of $1.04 \times 10^{-9} \text{ cm}^3/\text{sec}$ for formation of XeCl^* by Xe^* and Cl_2 reacting. The ArCl^* formation reaction-rate constant is calculated by using the 95 \AA^2 cross section that is reported by Piper et al. (Refs 54, 55) to be the Ar^* quenching cross section by Cl_2 . Golde and Thrush (Ref 7) state that more than 10% of Ar^* quenching by Cl_2 results in ArCl^* formation. Gundel et al. (Ref 56) state that approximately 50% of Ar^* quenching by Cl_2 results in ArCl^* formation. Therefore, taking 50% of the total quenching cross section and multiplying that number by the average relative velocity of Ar^* and Cl_2 results in a reaction-rate constant of $3.16 \times 10^{-10} \text{ cm}^3/\text{sec}$ for formation of ArCl^* by Ar^* reacting with Cl_2 .

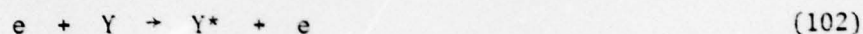
Conclusion. The harpoon reaction does seem to explain the formation of HgCl^* by Hg^* reacting with Cl_2 . Unfortunately,

this determination can be made only after the experimental data is gathered for the HgCl^* function cross section.

The remaining sections are all brief discussions about the development of several reaction-rate constants that are based on experimental data.

Secondary-Electron Excitation of Ar, Xe, and Hg

Introduction. Secondary-electron excitation of an atom is a reaction of the form in reaction 102.



The Y^* is an excited state which is long-lived and is called a metastable state.

The reaction-rate constant for excitation of Ar, Xe, and Hg by secondary electron impact are based on theoretical and experimental cross sections. The cross sections are approximated by straight lines of the form in equation 103, where ϵ is electron energy in eV and σ is the resultant cross section. The units of a and b are cm^2/eV and cm^2 , respectively.

$$\sigma = a\epsilon + b \quad (103)$$

The expectation value of $\langle \sigma v \rangle$ is calculated for a Maxwell-Boltzmann energy distribution of electrons with 4 eV average energy. Using $v = \left(\frac{2\epsilon}{m}\right)^{1/2}$ allows the integration limits to be zero energy to infinite energy as shown in equation 104.

$$\langle \sigma v \rangle = R_{\text{excitation}} = \int_0^{\infty} \frac{2}{\sqrt{\pi}} (kT)^{-3/2} \epsilon^{1/2} e^{-\epsilon/kT} \frac{\sqrt{\pi}}{m} \epsilon^{1/2} (a\epsilon + b) d\epsilon \quad (104)$$

The integration yields equation 105 which must be evaluated for the zero to infinite energy limits.

$$\begin{aligned} \langle \sigma v \rangle = & a \left[\frac{2^{3/2} \epsilon^2 e^{-\epsilon/kT}}{\sqrt{\pi m} (kT)^{1/2}} - \frac{2^{5/2} (kT)^{3/2}}{\sqrt{\pi m}} e^{-\epsilon/kT} \left(\frac{\epsilon}{kT} + 1 \right) \right] \\ & - b \left[\frac{2^{3/2} (kT)^{1/2}}{\sqrt{\pi m}} e^{-\epsilon/kT} \left(\frac{\epsilon}{kT} + 1 \right) \right] \end{aligned} \quad (105)$$

Ar and Xe. The Ar and Xe cross sections for electron-impact excitation to metastable states are the experimental values obtained by Schaper and Schiebner (Ref 57). The Ar cross section is approximated by equation 106.

$$\sigma = \begin{cases} 0 & , 0 \leq \epsilon \leq 11.55 \text{ eV} \\ 6.6666 \times 10^{-18} \epsilon - 7.7 \times 10^{-17} & , \epsilon > 11.55 \text{ eV} \end{cases} \quad (106)$$

The Xe cross section is approximated by equation 107.

$$\sigma = \begin{cases} 0 & , 0 \leq \epsilon \leq 8.08 \text{ eV} \\ 9.766 \times 10^{-18} \epsilon - 7.891 \times 10^{-17} & , \epsilon > 8.08 \text{ eV} \end{cases} \quad (107)$$

Substitution of equations 106 and 107 into equation 105 and evaluation over the proper limits yields electron-impact excitation reaction-rate constants of $1.62 \times 10^{-10} \text{ cm}^3/\text{sec}$ for Ar and $6.92 \times 10^{-10} \text{ cm}^3/\text{sec}$ for Xe.

Hg. The cross section for electron-impact excitation of Hg is limited to the excitation cross section for the $\text{Hg}^* (^3\text{P}_2)$ for reasons discussed in Chapter 2. Rockwood's (Ref 58) cross sections for excitation to various Hg states are the result of generating a self-consistent set of cross sections based on various experimental and calculated transport data. Rockwood (Ref 58) uses Borst (Ref 59) and von Engel (Ref 60) for his experimental data on excitation of $\text{Hg}^* (^3\text{P}_2)$. Unfortunately, none of the three authors' cross sections covers a large range of energy. The theoretical cross section of McConnell and Moiseiwitsch (Ref 61) is used in this calculation. McConnell and Moiseiwitsch (Ref 61) and Rockwell's (Ref 58) calculations are in good agreement. Both find a threshold for excitation to $\text{Hg}^* (^3\text{P}_2)$ at 5.7 eV and a maximum cross section of $3.2 \times 10^{-16} \text{ cm}^2$ at 6.4 eV. McDonnell and Moiseiwitsch's cross section is approximated in equation 108.

$$\sigma = \begin{cases} 0 & , 0 \leq \epsilon \leq 5.7, \epsilon > 17 \text{ eV} \\ 4.57143 \times 10^{-16} \epsilon - 2.60572 \times 10^{-15} & , 5.7 \leq \epsilon \leq 6.4 \text{ eV} \\ -0.3018868 \times 10^{-16} \epsilon + 5.1320755 \times 10^{-16} & , 6.4 \leq \epsilon \leq 17 \text{ eV} \end{cases} \quad (108)$$

The area under the curve generated by equation 108 is within 1.5% of the area under the curve of McConnell and Moiseiwitsch (Ref 61). Substitution of equation 108 into equation 105 and evaluation over the proper limits yields an electron-impact excitation reaction-rate constant of $8.45 \times 10^{-9} \text{ cm}^3/\text{sec}$ for excitation to $\text{Hg}^* (^3\text{P}_2)$.

Conclusion. The electron-impact excitation cross sections that are calculated in this section using a Maxwell-Boltzmann distribution for electron energies may be incorrect. The Maxwell-Boltzmann distribution of electron energies tends to skew the real distribution of electron energies toward the higher energies. Therefore, the reaction-rate constants that are calculated in this section are probably high.

Ionization of Excited States by Secondary-Electron Impact

Introduction. The ionization process by secondary electrons is generally in the form of reaction 109 where X^* is a metastable atom, X^+ is the ionized atom, and e is a secondary electron.



This process is a loss term for metastables and a gain term for secondary electrons and ions.

The ionization processes that are included are the ionization of Ar^* , Xe^* , and Hg^* . The cross sections for these processes are generated using equation 110. Equation 110 is an empirical expression for ionization cross sections of excited atoms and molecules that is developed by Vriens (Refs 62, 63).

$$\sigma = \frac{740 \pi a_0^2}{E + 3.25U} \left[\left(\frac{1}{U} - \frac{1}{E} \right) + \left(\frac{2U}{3} \right) \left(\frac{1}{U^2} - \frac{1}{E^2} \right) \right] \quad (110)$$

The cross section, σ , is a function of the electron energy E , in eV, the energy necessary to ionize the excited state U , in eV, and πa_0^2 which is equal to $0.88 \times 10^{-16} \text{ cm}^2$. The equation is fairly accurate for $U < 3.5 \text{ eV}$ (Ref 62). Gryzinski's (Ref 64) expression is more accurate for $U > 10 \text{ eV}$ (Ref 62).

The cross sections that are generated by Vriens' expression (Refs 62, 63) are approximated by straight lines as in equation 103. These expressions are substituted into equation 105 and evaluated over the proper limits of integration. The electrons are assumed to be given by a Maxwell-Boltzmann distribution with 4 eV average energy.

Ar*, Xe*, and Hg*. The following data is used in the calculations for the ionization of Ar*, Xe*, and Hg* by the secondary electrons. Assuming the Ar* is the lowest metastable state, the metastable energy is 11.548 eV. The ionization potential for ground state Ar is 15.75 eV (Ref 65). The resultant U is 4.211 eV. The equation describing the approximate cross section for Ar* ionization is given in equation 111.

$$\sigma = \begin{cases} 0 & , 0 < \epsilon < 4.211 \text{ eV} \\ \{ 3.6882 \times 10^{-16} \epsilon - 1.5531 \times 10^{-15} \} & , 4.211 < \epsilon < 6.1089 \text{ eV} \\ 7 \times 10^{-16} & , \epsilon > 6.1089 \text{ eV} \end{cases} \quad (111)$$

Assuming Xe* is in the lowest metastable state, the metastable energy is 8.315 eV. The ionization potential for ground state Xe is 12.129 eV (Ref 65). The resultant U is 3.814 eV. The equations

describing the approximate cross section for Xe* ionization are given in equation 112.

$$\sigma = \begin{cases} 0 & , 0 < \epsilon < 3.814 \text{ eV} \\ 5.9677 \times 10^{-16} - 2.2761 \times 10^{-15} \epsilon & , 3.814 < \epsilon < 5.322 \text{ eV} \\ 9 \times 10^{-16} & , \epsilon > 5.322 \text{ eV} \end{cases} \quad (112)$$

The Hg* is considered to be in the 3P_2 metastable state for reasons discussed in Chapter 2. The excitation energy of Hg* (3P_2) is 5.434 eV, and the ground state ionization potential of Hg is 11.434 eV (Ref 66). The resultant U is 5.00 eV. The equations describing the approximate cross section for Hg* ionization are given in equation 113.

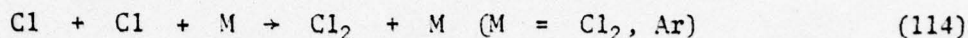
$$\sigma = \begin{cases} 0 & , 0 < \epsilon < 5.0 \text{ eV} \\ 2.48 \times 10^{-16} - 1.24 \times 10^{-15} \epsilon & , 5.0 < \epsilon < 7.097 \text{ eV} \\ 5.2 \times 10^{-16} & , \epsilon > 7.097 \text{ eV} \end{cases} \quad (113)$$

Conclusions. The reaction-rate constants for ionization of Ar* , Xe* , and Hg* are $3.27 \times 10^{-8} \text{ cm}^3/\text{sec}$, $4.83 \times 10^{-8} \text{ cm}^3/\text{sec}$, and $1.94 \times 10^{-8} \text{ cm}^3/\text{sec}$, respectively. Again, these reaction-rate constants are probably too high, because the Maxwell-Boltzmann distribution is used to describe the electron energies.

Bauer and Bartky (Refs 67, 68) present classical methods for calculating cross sections for both excitation and ionization by electron-impact.

Cl-Cl Recombination Reactions

The two Cl-Cl atom recombination reactions included in this model are of the form in reaction 114.



The reaction-rate constants for this model are the result of experimental data obtained by Clyne and Stedman (Ref 69). This data implies that equation 115 gives the reaction-rate constant for reaction 114 with Cl_2 as the third body. The temperature T is in units of $^\circ \text{K}$.

$$R = 10^{16.3} \left(\frac{T}{300}\right)^{-2.7} \text{ cm}^6 \text{ mole}^{-2} \text{ sec}^{-1} \quad (115)$$

Substituting the temperature for this model, 533°K , into equation 115 results in a reaction-rate constant of $4.227 \times 10^{15} \text{ cm}^6 \text{ mole}^{-2} \text{ sec}^{-1}$ for Cl_2 as a third body. This reaction-rate constant converts to $1.165 \times 10^{-32} \text{ cm}^6/\text{sec}$.

The data from Clyne and Stedman's work (Ref 69) implies that equation 116 gives the reaction-rate constant for reaction 114 with Ar as a third body.

$$R = 10^{15.6} \left(\frac{T}{300}\right)^{-3.0} \text{ cm}^6 \text{ mole}^{-2} \text{ sec}^{-1} \quad (116)$$

Again, temperature, T , is in $^\circ \text{K}$. Substitution of the temperature for the model, 533°K , into equation 116 results in a reaction-rate constant of $7.099 \times 10^{14} \text{ cm}^6 \text{ mole}^{-2} \text{ sec}^{-1}$. This reaction-rate constant converts to $1.957 \times 10^{-33} \text{ cm}^6/\text{sec}$ for reaction 114 with Ar as the third body.

The value found for reaction with Ar as the third body by Clyne and Stedman (Ref 69) is in good agreement with the values found by Hutton and Wright (Ref 70) and Bader and Ogryzlo (Ref 71). Clyne and Stedman's value for Ar as a third body in reaction 114 is $(4.4 \pm 0.5) \times 10^{15} \text{ cm}^6 \text{mole}^{-2} \text{sec}^{-1}$ at 298° K (Ref 69). Hutton and Wright's value for the same reaction at 300° K is $(4.25 \pm 0.8) \times 10^{15} \text{ cm}^6 \text{mole}^{-2} \text{sec}^{-1}$ (Ref 70). Bader and Ogryzlo's value for this reaction at 313° K is $4 \times 10^{15} \text{ cm}^6 \text{mole}^{-2} \text{sec}^{-1}$ (Ref 71).

Radiative Decay of ArCl*, XeCl*, and HgCl*

The radiative lifetimes that are used in this model for ArCl* and XeCl* are based on experimental data. Gundel et al. (Ref 56) estimate the radiative lifetime of ArCl* to be 20 ns at higher pressures. At pressures of 1 to 2 torr, Gundel et al. (Ref 56) estimate the lifetime of ArCl* to be 100 ns. Hart and Searles (Ref 72) estimate the radiative lifetime of XeBr* to be 17.5 ns. Dunning and Hay (Ref 73) calculate the radiative lifetime of KrF* to be 6.5 ns. These radiative lifetimes are used as guidance to estimate the radiative lifetimes of ArCl* and XeCl* to be 20 ns. These radiative lifetimes lead to reaction-rate constants of $5 \times 10^7 \text{ sec}^{-1}$ for the bound-free radiative decay of ArCl* (Ref 56) and XeCl* to their products of Ar and Cl and Xe and Cl, respectively.

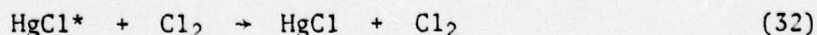
The radiative lifetime of HgCl* is reported to be 40 ns (Ref 8). This radiative lifetime for HgCl* leads to a reaction-rate constant of $2.5 \times 10^7 \text{ sec}^{-1}$ for the radiative decay of HgCl*. The HgCl* decays to a bound state of HgCl.

Ionization and Excitation by Electron Beam

The cross sections for ionization and excitation of Ar and Xe by electron-beam electrons are provided by Hunter (Ref 5). These cross sections are calculated by multiplying 2.4 times the Berger-Seltzer cross sections (Ref 74). The 2.4 factor is a compensation factor for scattering losses. The total cross section is then partitioned so that approximately 75% results in ionization and 25% results in excitation of Ar and Xe. For the beam electron energy that is used in Chapter 4, the cross section for ionization of Ar is $7.68 \times 10^{-18} \text{ cm}^2$; the cross section for excitation of Ar to a metastable state is $2.11 \times 10^{-18} \text{ cm}^2$; the cross section for ionization of Xe is $1.90 \times 10^{-17} \text{ cm}^2$; and the cross section for excitation of Xe to a metastable state is $6.33 \times 10^{-18} \text{ cm}^2$. Other work on ionization sections for Ar is provided in References 75 and 76, and does agree fairly well with Berger and Seltzer (Ref 74).

HgCl* Quenching

The only reaction that is included in this model for the quenching of HgCl* is reaction 32.



The reaction-rate constant for this reaction is similar to that for XeBr* quenching by Br₂ and KrF* quenching by F₂. The reaction-rate constant for XeBr* quenching by Br₂ is $(8 \pm 2) \times 10^{-10} \text{ cm}^3/\text{sec}$ (Ref 72). The reaction-rate constant for KrF* quenching by F₂ is

1×10^{-9} cm³/sec (Ref 77). The reaction-rate constant for HgCl* by Cl₂ is reported to be 5.62×10^{-10} cm³/sec (Ref 8). This reported value is the quenching reaction-rate constant used in this model.

The difference between quenching of both XeBr* by Br₂ and KrF* by F₂ and HgCl* by Cl₂ is that a bound state exists for HgCl, but does not exist for XeBr and KrF. All HgCl* appears to be quenched to a bound state of HgCl (Ref 8).

Summary

The reaction-rate constants that are developed in this section are based on both theoretical and experimental data. Table 2 shows the reactions and reaction-rate constants that are used in the solution of this model that is presented in Chapter 4.

Table II
Reactions & Reaction-Rate Constants

<u>Reaction</u>	<u>Equation Number</u>	<u>Reference</u>	<u>Reaction-Rate Constant</u>
$e + \text{Ar}_2^+ \rightarrow \text{Ar}^* + \text{Ar}$	Text	17	3.9×10^{-8} cm ³ /sec
$e + \text{Xe}_2^+ \rightarrow \text{Xe}^* + \text{Xe}$	Text	18	8.16×10^{-8} cm ³ /sec
$e + \text{Cl}_2 \rightarrow \text{Cl}^- + \text{Cl}$	Text	23	3.7×10^{-9} cm ³ /sec
$\text{Ar}^+ + 2\text{Ar} \rightarrow \text{Ar}_2^+ + \text{Ar}$	Text	31	2.5×10^{-31} cm ⁶ /sec
$\text{Xe}^+ + \text{Xe} + \text{Ar} \rightarrow \text{Xe}_2^+ + \text{Ar}$	77b	27	4.96×10^{-31} cm ⁶ /sec
$\text{Xe}^+ + \text{Xe} + \text{Xe} \rightarrow \text{Xe}_2^+ + \text{Xe}$	Text	31	3.6×10^{-31} cm ⁶ /sec
$\text{Ar}_2^+ + \text{Xe} \rightarrow \text{Xe}^+ + 2\text{Ar}$	83	36	6.65×10^{-10} cm ³ /sec
$\text{Xe}_2^+ + \text{Hg} \rightarrow \text{Hg}^+ + 2\text{Xe}$	83	36	3.11×10^{-10} cm ³ /sec
$\text{Ar}^+ + \text{Cl}^- \rightarrow \text{ArCl}^*$	97a	33	2.13×10^{-6} cm ³ /sec
$\text{Xe}^+ + \text{Cl}^- \rightarrow \text{XeCl}^*$	97a	33	1.75×10^{-6} cm ³ /sec

Table II (Cont'd)

Reaction	Equation Number	Reference	Reaction-Rate Constant
$\text{Hg}^+ + \text{Cl}^- \rightarrow \text{HgCl}^*$	97a	53	$1.685 \times 10^{-6} \text{ cm}^3/\text{sec}$
$\text{Hg}^* + \text{Cl}_2 \rightarrow \text{HgCl}^* + \text{Cl}$	Text	5	$4.18 \times 10^{-10} \text{ cm}^3/\text{sec}$
$\text{Xe}^* + \text{Cl}_2 \rightarrow \text{XeCl}^* + \text{Cl}$	Text	52	$1.04 \times 10^{-9} \text{ cm}^3/\text{sec}$
$\text{Ar}^* + \text{Cl}_2 \rightarrow \text{ArCl}^* + \text{Cl}$	Text	54,55	$3.16 \times 10^{-10} \text{ cm}^3/\text{sec}$
$e + \text{Ar} \rightarrow \text{Ar}^* + e$	105,106	57	$1.62 \times 10^{-10} \text{ cm}^3/\text{sec}$
$e + \text{Xe} \rightarrow \text{Xe}^* + e$	105,106	57	$6.92 \times 10^{-10} \text{ cm}^3/\text{sec}$
$e + \text{Hg} \rightarrow \text{Hg}^* + e$	105,108	61	$8.45 \times 10^{-9} \text{ cm}^3/\text{sec}$
$e + \text{Ar}^* \rightarrow \text{Ar}^+ + 2e$	105,111	62	$3.27 \times 10^{-8} \text{ cm}^3/\text{sec}$
$e + \text{Xe}^* \rightarrow \text{Xe}^+ + 2e$	105,112	62	$4.83 \times 10^{-8} \text{ cm}^3/\text{sec}$
$e + \text{Hg}^* \rightarrow \text{Hg}^+ + 2e$	105,113	62	$1.94 \times 10^{-8} \text{ cm}^3/\text{sec}$
$\text{Cl} + \text{Cl} + \text{Cl}_2 \rightarrow 2\text{Cl}_2$	115	69	$1.165 \times 10^{-32} \text{ cm}^6/\text{sec}$
$\text{Cl} + \text{Cl} + \text{Ar} \rightarrow \text{Cl}_2 + \text{Ar}$	116	69	$1.957 \times 10^{-33} \text{ cm}^6/\text{sec}$
$\text{ArCl}^* \rightarrow \text{Ar} + \text{Cl} + h\nu$	Text	56	$5 \times 10^7 \text{ sec}^{-1}$
$\text{XeCl}^* \rightarrow \text{Xe} + \text{Cl} + h\nu$	Text	Text	$5 \times 10^7 \text{ sec}^{-1}$
$\text{HgCl}^* \rightarrow \text{HgCl} + h\nu$	Text	8	$2.5 \times 10^7 \text{ sec}^{-1}$
$e^{\text{P}} + \text{Ar} \rightarrow \text{Ar}^+ + e^{\text{P}} + e$	Text	5	
$e^{\text{P}} + \text{Ar} \rightarrow \text{Ar}^* + e$	Text	5	
$e^{\text{P}} + \text{Xe} \rightarrow \text{Xe}^+ + e^{\text{P}} + e$	Text	5	
$e^{\text{P}} + \text{Xe} \rightarrow \text{Xe}^* + e^{\text{P}}$	Text	5	
$\text{HgCl}^* + \text{Cl}_2 \rightarrow \text{HgCl} + \text{Cl}_2$	Text	8	$5.62 \times 10^{-10} \text{ cm}^3/\text{sec}$

The reaction-rate constants for the excitation of Ar, Xe, and Hg and the ionization of Ar*, Xe*, and Hg* by secondary electrons

may need to be adjusted in Chapter 4. The assumption that the secondary electrons are in a Maxwell-Boltzmann distribution with an average energy of 4 eV is probably incorrect.

IV. Solution and Analysis

Overview

In this chapter, the rate equations for the various species that are presented in Chapter 2 are used to determine solutions for two cases of this model. The first case that is investigated involves the reaction kinetics of a HgCl laser that is generated by an electron beam only. The second case involves the reaction kinetics of a HgCl laser that is initiated by an electron beam, and the lasing plasma is subjected to an applied d.c. electric field.

A computer program supplied by A. M. Hunter (Ref 5) is used to analyze both cases for various electron beam currents and reaction-rate constant sensitivities. This program uses a numerical integrator to solve the rate equations. The integrator solves for the change in number densities of the various species by stepping forward in time by a small time interval and adding or subtracting the increase or decrease in number densities to the appropriate number densities for each species at the beginning of the small time interval.

Initial computer program runs did not indicate a stable plasma could be maintained for the discharge-sustained HgCl laser simulation. This problem is caused by the inaccurate assumption that the secondary electrons can be described by a Maxwell-Boltzmann energy distribution. This problem is solved by adjusting the reaction-rate constants for excitation of Ar and Xe by secondary electron impact and for ionization of Ar* and Xe* by secondary electron impact. By adjusting these reaction-rate

constants to the constants used for the same reactions in the KrF laser, a stable plasma is achieved for the discharge-sustained HgCl laser simulation. The constants that are used for the solution in this chapter are 6.62×10^{-12} cm³/sec for excitation of Ar by secondary electrons, 7.46×10^{-8} cm³/sec for ionization of Ar* by secondary electrons, 7.75×10^{-11} cm³/sec for excitation of Xe by secondary electrons, and 1.16×10^{-7} cm³/sec for ionization of Xe* by secondary electrons. These constants are provided by A. M. Hunter (Ref 5) and eliminate the problems for these reactions that are caused by assuming a Maxwell-Boltzmann distribution for the secondary electrons. The Maxwell-Boltzmann distribution contains more higher energy secondary electrons than the actual secondary electron energy distribution (Ref 5).

This chapter is developed in the following manner. First, a determination is made to find which species number densities vary slowly with time and can be considered constant. Second, an analytical solution of this model with no applied electric field is presented for the electron density and is compared to the computer solution. Third, an analytical solution of this model with an applied electric field is presented for the electron density and is compared to the computer solution. The primary emphasis is placed on the electron number density, because the electron number density is found to determine the stability of the e-beam sustained KrF laser (Ref 5) and is assumed to determine the stability of the HgCl laser in a similar manner.

Slow Varying Species

Before an analytical solution is found for this model, the species number densities that vary slowly are determined. A species number

density that is found to vary slowly can be assumed to be constant in the analytical solution.

A species number density is considered to vary slowly if the initial lifetime for an atom or molecule of a species is greater than 10^{-6} seconds. The average initial lifetime for an atom or molecule is determined by dividing the initial \dot{n}_i by the initial number density of the species. The resultant number is approximately equal to the inverse of initial lifetime. This relationship is shown in equation 117.

$$\frac{\dot{n}_i}{n_i} = \frac{1}{T_i} \quad (117)$$

The only species that exist at time zero are Ar , Xe , Hg , Cl₂ , and e^p . All other species number densities are initially zero. Therefore, the only species with an initial lifetime are Ar , Xe , Hg , Cl₂ , and electrons.

The Ar , Xe , Hg , Cl₂ , and electrons initial lifetimes are found in the following manner. First, the \dot{n}_i is found by solving equations 35, 36, 37, 44, and 47 for the applicable species i . The n_i for Ar , Xe , Hg , and Cl₂ are $3.726 \times 10^{19} \text{ cm}^{-3}$ for Ar , $4.531 \times 10^{18} \text{ cm}^{-3}$ for Xe , $1.745 \times 10^{18} \text{ cm}^{-3}$ for Hg , and $9.062 \times 10^{16} \text{ cm}^{-3}$ for Cl₂ . The n_i that is used in equation 117 for electrons is the number density for electron beam electrons only. The initial lifetimes for Ar , Xe , Hg , and Cl₂ are found to be greater than 10^{-6} seconds for electron beam currents to 15 amps/cm² . The initial lifetime for electrons is found to be less than 10^{-6} seconds for all electron beam currents greater than 1 amp/cm² . Therefore, the number

densities for Ar , Xe , Hg , and Cl₂ are considered constant in the analytical solution. The number density of electrons is not considered constant in the analytical solution.

Solution for HgCl Laser Without Applied Electric Field

Introduction and assumptions. The analytical solution for the electron number density is based on two major assumptions. One smaller assumption is made in the development of this solution. This solution is done for a 5 amp/cm² electron beam current and an initial gas mixture of 3.726×10^{19} Ar atoms/cm³ , 4.531×10^{18} Xe atoms/cm³ , 1.745×10^{18} Hg atoms/cm³ , and 9.062×10^{16} Cl₂ molecules/cm³ . The reaction-rate constants that are used in this solution are those reaction-rate constants that are presented to this point in this paper.

The primary assumption that is made for the analytical solution of the HgCl laser without an applied electric field is that the secondary electrons are in thermal equilibrium with the surrounding gas. This simplifying assumption is not completely true, because it does not include the effect of thermalizing the secondary electrons that start at a higher than thermal energy. A true distribution of these secondary electrons can be found by solving the Boltzmann equation, but is beyond the scope of this paper. This assumption of thermal electrons changes the dissociative-recombination reaction-rate constants for Ar₂⁺ (reaction 10) and Xe₂⁺ (reaction 21) to 5.99×10^{-7} cm³/sec and 1.88×10^{-6} cm³/sec , respectively (Refs 17, 18). These increases are due to the decrease in secondary electron temperature.

A second assumption that is made in the analytical solution of the HgCl laser without an applied electric field is that the secondary electrons are not energetic enough to excite Hg, Ar, or Xe to their metastable states and are not energetic enough to ionize the excited states of Hg*, Ar*, and Xe*. Therefore, the reaction-rate constants for reactions 15 through 20 are set equal to zero. This assumption is not totally correct, because the effect of thermalizing the secondary electrons that start at higher than thermal energies is not included in this analysis.

The third assumption that is made in this solution is that an equilibrium electron number density exists for at least 1×10^{-6} seconds and that equilibrium number densities exist for all other species. This assumption is almost accurate, because these number densities do in fact vary slowly after they are initially established for all species. Also, the equilibrium electron number density is assumed to be much less than 5.0×10^{15} electrons/cm³.

Analytical solution. The analytical solution is a result of the solution of equations 35, 38, 39, 40, and 41. The equilibrium number density of electrons is found by setting \dot{n}_e equal to zero and solving for n_e . The n_e is found to be dependent on $n_{Xe_2^+}$ and $n_{Ar_2^+}$. By setting equation 41 equal to zero, $n_{Ar_2^+}$ is found to be equation 118, if n_{Ar^+} and n_e are in cm⁻³.

$$n_{Ar_2^+} = \frac{(3.471 \times 10^8) n_{Ar^+}}{(3.013 \times 10^3) + (5.99 \times 10^{-7}) n_e} \text{ cm}^{-3} \quad (118)$$

AD-A055 229

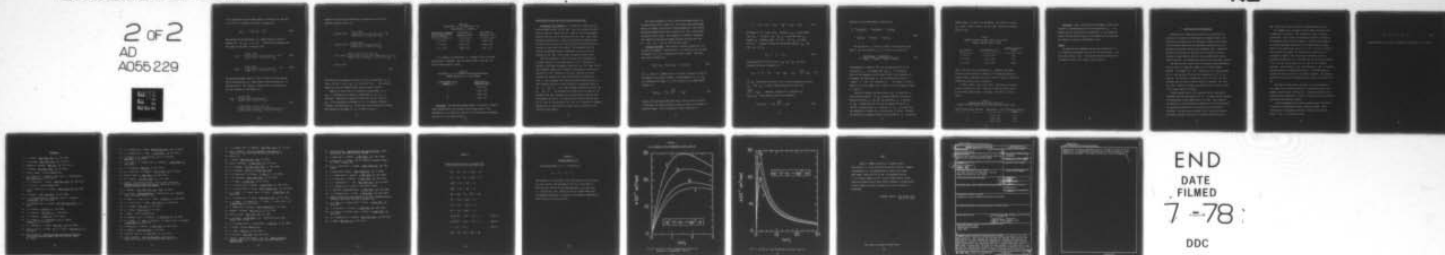
AIR FORCE INST OF TECH WRIGHT-PATTERSON AFB OHIO SCH--ETC F/G 20/5
REACTION-R CONSTANTS AND SIMPLE RATE THEORIES APPLIED TO THE ME--ETC(U)
MAR 78 R P SUMMERS

UNCLASSIFIED

AFIT/GNE/PH/78M-9

NL

2 OF 2
AD
A055 229



END
DATE
FILMED
7-78
DDC

If the equilibrium electron number density is assumed to be less than $5.0 \times 10^{15} \text{ cm}^{-3}$, equation 118 reduces to equation 119.

$$n_{\text{Ar}_2^+} \approx 0.1152 n_{\text{Ar}^+} \text{ cm}^{-3} \quad (119)$$

The solution for the equilibrium Ar^+ number density is given in equation 120. The n_{Cl^-} is in cm^{-3} . Substitution of equation 120 into equation 119 results in equation 119a.

$$n_{\text{Ar}^+} = \frac{(8.942 \times 10^{21})}{(3.471 \times 10^8) + (2.134 \times 10^{-6}) n_{\text{Cl}^-}} \text{ cm}^{-3} \quad (120)$$

$$n_{\text{Ar}_2^+} \approx \frac{(1.03 \times 10^{21})}{(3.999 \times 10^7) + (2.458 \times 10^{-7}) n_{\text{Cl}^-}} \text{ cm}^{-3} \quad (119a)$$

The equilibrium number density of Xe_2^+ is found by solving equation 38 for the equilibrium Xe^+ number density and substituting the Xe^+ solution into the Xe_2^+ equation. Equation 119a is substituted into the Xe_2^+ solution to give equation 121.

$$n_{\text{Xe}_2^+} = \frac{(9.113 \times 10^7)}{(5.427 \times 10^8) + (1.88 \times 10^{-6}) n_e} \quad (121)$$

$$\left[\frac{(3.211 \times 10^{30}) + (6.61 \times 10^{14}) n_{\text{Cl}^-}}{(3.644 \times 10^{15}) + 92.38 n_{\text{Cl}^-} + (4.3 \times 10^{-13}) n_{\text{Cl}^-}^2} \right]$$

Equations 121 and 119a are substituted into equation 35 to give the quadratic equation 122 for n_e .

$$\begin{aligned}
 & [(6.298 \times 10^2) - \frac{(1.16 \times 10^9)}{(3.999 \times 10^7) + (2.458 \times 10^{-7}) n_{Cl^-}}] n_e^2 \\
 & + [(2.037 \times 10^{17}) - \frac{(3.348 \times 10^{23})}{(3.999 \times 10^7) + (2.458 \times 10^{-7}) n_{Cl^-}}] n_e \\
 & - (1.71 \times 10^2) \left\{ \frac{(3.211 \times 10^{30}) + (6.61 \times 10^{14}) n_{Cl^-}}{(3.644 \times 10^{15}) + 92.38 n_{Cl^-} + (4.3 \times 10^{-13}) n_{Cl^-}^2} \right\} n_e \\
 & - (6.313 \times 10^{30}) \\
 & = 0
 \end{aligned} \tag{122}$$

The solution of the quadratic equation 122 yields an equilibrium n_e of $3.683 \times 10^{13} \text{ cm}^{-3}$ for an n_{Cl^-} of $6.488 \times 10^{13} \text{ cm}^{-3}$. This solution agrees well with the computer results that are shown in Table 3.

Equation 122 also results in a decrease in equilibrium n_e as n_{Cl^-} is increased and an increase in equilibrium n_e as n_{Cl^-} is decreased. Examination of equation 48 shows that the only source of n_{Cl^-} is the dissociative attachment of Cl_2 by secondary electrons. Therefore, the equilibrium n_e is sensitive to the reaction-rate constant for dissociative attachment of Cl_2 as shown in Table 3.

Table III
Equilibrium n_e as a Function of n_{Cl^-}
Beam Current is 5 amp/cm².

Dissociative Attachment Reaction-Rate Constant for Cl ₂ (cm ³ /sec)	Equilibrium n_{Cl^-} Population (cm ⁻³)	Equilibrium n_e Population (cm ⁻³)
1.0×10^{-8}	7.717×10^{13}	1.439×10^{13}
3.7×10^{-9}	6.488×10^{13}	3.809×10^{13}
1.0×10^{-10}	4.889×10^{12}	5.487×10^{14}

As is expected, the equilibrium n_e increases as the initiating beam current is increased. This is shown in Table 4 where only the electron beam current is varied.

Table IV
Equilibrium n_e as a Function of Electron Beam Current
Computer Solution at 1×10^{-6} Seconds

Electron Beam Current (amp/cm ²)	Equilibrium n_e Population (cm ⁻³)
1	7.032×10^{12}
2	1.394×10^{13}
5	3.809×10^{13}
10	7.891×10^{13}

Conclusion. The equilibrium number density of electrons is approximately proportional to the incident electron beam current. This equilibrium n_e is also fairly sensitive to the dissociative attachment rate for Cl₂ as is shown in Table 3.

Solution for the HgCl Laser with Applied Electric Field

Introduction and assumptions. The analytical solution for the electron number density for the HgCl laser with an applied electric field is done for a beam current of 1 amp/cm^2 and the same number densities that are used in the solution for the HgCl laser without an applied electric field. Again, the reaction-rate constants that are used in this solution are those reaction-rate constants that are presented to this point in this paper. The assumptions for this solution are different from the assumptions that are used in the solution for the HgCl laser without an applied electric field.

The first assumption is that the electric field maintains the secondary electrons at an average energy of 4 eV. This number is similar to the energy of secondary electrons in the KrF laser (Ref 5). This assumption changes the dissociative recombination reaction-rate constants for Ar_2^+ (reaction 10) and Xe_2^+ (reaction 21) to the reaction-rate constants for these reactions that are presented in Table 2. This assumption also means that enough energy now exists in some secondary electrons to cause excitation to metastable states of Hg, Ar, and Xe. Also, some secondary electrons can ionize Hg^* , Ar^* , and Xe^* . The reaction-rate constants that are used for Hg excitation and Hg^* ionization are the reaction-rate constants that are presented in Table 2. The reaction-rate constants that are used for Ar and Xe excitation and Ar^* and Xe^* ionization by secondary electrons are the reaction-rate constants that are presented in the overview of this chapter.

The second assumption is that an equilibrium number density for all species does exist at some time. The electron equilibrium number density is assumed to be within an order-of-magnitude of the electron equilibrium number density that is found for the HgCl laser without an applied electric field. This assumption is probably a reasonable one, because the same species number densities are being used, and Ar , Hg , Cl₂ , and Xe still all very slowly.

Analytical solution. This solution is based on equation 35, the electron rate equation. The first step is to investigate the loss terms of equation 35 to see if a dominant loss term is found. These terms are listed in equation 123.

$$- R_{9a} n_e n_{Cl_2} - R_{10} n_e n_{Ar_2^+} - R_{21} n_e n_{Xe^+} \quad (123)$$

The n_e factor is a common factor to all terms in equation 123 and can be ignored for the present argument. By approximating R_{21} as $2R_{10}$ and eliminating the common n_e factor, equation 123 is approximately equation 124.

$$- R_{9a} n_{Cl_2} - 2R_{10} \left(\frac{n_{Ar_2^+}}{2} + n_{Xe^+} \right) \quad (124)$$

Because the entire plasma maintains overall neutral state and charge is conserved, the number of negative charges is equal to the number of positive charges. This relationship is shown in equation 125.

$$n_e + n_{Cl^-} = n_{Ar^+} + n_{Xe^+} + n_{Hg^+} + n_{Ar_2^+} + n_{Xe_2^+} \quad (125)$$

The number of Cl_2 varies slowly. Therefore, n_{Cl_2} is much greater than n_{Cl^-} . The sum of n_{Cl^-} and n_e is much less than n_{Cl_2} , because n_e is probably about 10^{13} cm^{-3} , and n_{Cl_2} is almost 10^{17} cm^{-3} . Equation 126 shows the relationship between n_{Cl_2} and both n_{Cl^-} and n_e .

$$n_{Cl_2} \gg n_e + n_{Cl^-} \quad (126)$$

Solving equation 125 for the sum of $n_{Ar_2^+}$ and $n_{Xe_2^+}$ and using equation 126 results in equation 127.

$$n_{Cl_2} \gg n_e + n_{Cl^-} - n_{Xe^+} - n_{Hg^+} - n_{Ar^+} > \frac{n_{Ar_2^+}}{2} + n_{Xe_2^+} \quad (127)$$

The R_{9a} reaction-rate constant is only an order-of-magnitude less than R_{10} , and n_{Cl_2} is several orders-of-magnitude greater than

$\left(\frac{n_{Ar_2^+}}{2} + n_{Xe_2^+}\right)$. Therefore, equation 128 is reasonable and

$R_{9a} n_e n_{Cl_2}$ is the dominant electron loss mechanism.

$$R_{9a} n_e n_{Cl_2} \gg 2R_{10} \left(\frac{n_{Ar_2^+}}{2} + n_{Xe_2^+}\right) \quad (128)$$

Equation 35 is now approximated by equation 35a.

$$\begin{aligned} \dot{n}_e = & V_{eb} \sigma_{Ar} n_{eb} n_{Ar} + V_{eb} \sigma_{Xe} n_{eb} n_{Xe} + R_{16} n_e n_{Hg^*} \\ & + R_{18} n_e n_{Ar^*} + R_{20} n_e n_{Xe^*} - R_{9a} n_e n_{Cl_2} \end{aligned} \quad (35a)$$

The equilibrium n_e solution is found by setting equation 35a equal to zero and solving for n_e as is shown in equation 129.

$$n_e = \frac{V_{eb} \sigma_{Ar} n_{eb} n_{Ar} + V_{eb} \sigma_{Xe} n_{eb} n_{Xe}}{R_{9a} n_{Cl_2} - (R_{16} n_{Hg^*} + R_{18} n_{Ar^*} + R_{20} n_{Xe^*})} \quad (129)$$

The denominator of equation 129 is the determining factor for the equilibrium n_e . By assuming that $R_{9a} n_{Cl_2}$ is the dominant factor in the denominator and the other terms in the denominator can be ignored, the equilibrium n_e for an electron beam current of 1 amp/cm² is 6.937×10^{12} electrons cm⁻³. This number is within a factor of 1.5 of the number that is found by using the computer program at 1 amp/cm².

Analysis of equation 129 shows that as R_{9a} is varied the n_e grows larger or smaller. If R_{9a} is smaller than the value that is reported by Sides et al. (Ref 23), the equilibrium n_e is greater. If R_{9a} is larger than the value that is reported by Sides et al. (Ref 23), the equilibrium n_e is smaller. If R_{9a} is so small that the denominator is almost zero, no equilibrium n_e exists. Therefore, the dissociative-attachment reaction-rate constant for Cl_2 at electron

energies about 4 eV needs to be determined. The effects of various R_{9a} values is shown in Table 5 for the HgCl laser with an applied electric field.

Table V
Computer Solution for HgCl Laser and R_{9a} Varied
1 amp/cm² Applied Electric Field

R_{9a} (cm ³ /sec)	Equilibrium n_e (cm ⁻³)	Discharge Transition (nsec)
1.0×10^{-10}	8.672×10^{13}	32.3
3.7×10^{-9}	1.172×10^{13}	224
1.0×10^{-8}	4.775×10^{12}	> 1000

Table 5 shows that, as the equilibrium n_e increases, the plasma stability is more difficult to maintain. The discharge transition column in Table 5 indicates the time at which the plasma is definitely unstable and lasing action is destroyed.

A similar effect to that of the HgCl laser without an applied field is found for the HgCl laser with an applied electric field as the electron beam current is increased. The effect is shown in Table 6.

Table VI
Computer Solution for HgCl Laser with
1 amp/cm² Applied Electric Field and Electron Beam Current Varied

Electron Beam Current (amp/cm ²)	Equilibrium n_e (cm ⁻³)	Discharge Transition (nsec)
1	1.172×10^{13}	224
2	2.180×10^{13}	93.7
5	6.122×10^{13}	41.4

Conclusion. Again, the dissociative-attachment reaction-rate constant is a determining factor for the equilibrium n_e . The applied electric field raises the equilibrium n_e and causes the plasma to become unstable sooner by the addition of electrons that are created by ionization of metastable states.

Summary

The dissociative-attachment reaction-rate constant for Cl_2 is an important determining factor in both the equilibrium n_e and the plasma stability time. The electron population appears to be an important factor in the overall plasma stability.

V. Conclusions and Recommendations

Several factors concerning the model that is constructed and analyzed in this paper are interesting for different reasons. The reaction-rate constants that are developed in Chapter 3 are examples of the excellent theoretical and experimental predictions that can be made by using simple theories and experimental data. Theoretical reaction-rate constants are predicted for ion-neutral association reactions, charge transfer reactions, ionic recombination, and harpooning reactions. The theoretical predictions give reasonable results.

The reaction-rate constants that are presented using experimental data as a basis are sometimes incomplete or in need of further research. For example, the ArCl^* formation by Ar^* being quenched by Cl_2 only includes 50% of the total quenching of Ar^* by Cl_2 (Ref 56). The radiative lifetimes for ArCl^* and XeCl^* are only estimates that are based on similar radiative lifetimes. The ArCl^* and XeCl^* radiative lifetimes are probably within a factor of three of the actual radiative lifetimes.

Further research needs to be conducted into the dissociative-attachment reaction-rate constant for Cl_2 at higher electron energies. The equilibrium electron number density and HgCl laser stability are sensitive to this reaction-rate constant at all electron energies. The majority of research for this reaction is done for thermal electrons. The reaction-rate constant that is used in this model is for thermal electrons (Ref 23) and is probably inaccurate for the

HgCl laser analysis that is done for an applied electric field.

The assumption of a secondary electron energy distribution that is Maxwellian is incorrect. This assumption is made to simplify calculations. Many of these calculations are adjusted in Chapter 4. The adjustments that are made in Chapter 4 show that the assumption of a Maxwell-Boltzmann distribution for secondary electron energy forces to the reaction-rate constants that are calculated in Chapter 3 for excitation to be high. The reaction-rate constants that are calculated in Chapter 3 for ionization of metastable states by secondary electrons are low. Corrections are only made for excitation of Ar and Xe and ionization of Ar* and Xe* by secondary electrons. The excitation of Hg and ionization of Hg* by secondary electrons needs to be investigated further. A Boltzmann equation solution for these reactions is one possible approach. This approach possibly can be used to investigate primary electron interaction with Hg .

One aspect of high-energy lasers that is not investigated in this paper is the initial distribution of vibrational states of the primary electron energy absorbing gas. A possible dependence exists between the gas temperature, the initial vibrational state distribution, and several reaction-rate constants.

A final recommendation for future research concerns the effect of pressure on thermolecular charge transfer reactions. These reactions are of the general form that is shown in reaction 130 where X and Y are different atoms.

$$X_2^+ + Y_2 + X + Y_2^+ + 3X \quad (130)$$

Recent research in this area is presented in References 78, 79, and 80.

References

1. J. H. Parks. Appl. Phys. Lett., 31: 192 (1977).
2. J. Gary Eden. Appl. Phys. Lett., 31: 448 (1977).
3. Frederick G. Gebhardt. Appl. Opt., 15: 1479 (1976).
4. K. Wieland. Helv. Phys. Acta., 14: 420 (1941).
5. Allen M. Hunter. Private communication.
6. H. F. Krause, S. G. Johnson, S. Datz, and F. K. Schmidt-Bleck. Chem. Phys. Lett., 31: 577 (1975).
7. M. F. Golde and B. A. Thrush. Chem. Phys. Lett., 29: 486 (1974).
8. R. O. Hunter. Private communication.
9. M. A. A. Clyne and D. H. Stedman. Trans. Farad. Soc., 64: 2698 (1968).
10. S. Mrozowski. Rev. Mod. Phys., 16: 153 (1944).
11. A. A. Christodoulides, R. Schumacher, and R. N. Schindler. J. Chem. Phys., 79: 1904 (1975).
12. J. N. Bardsley and M. A. Biondi. Adv. Atom. Mole. Phys., 6: 1 (1970).
13. J. N. Bardsley. J. Phys. B., 1: 349 (1968).
14. J. N. Bardsley. Phys. Rev. A., 2: 1359 (1970).
15. J. N. Bardsley. J. Phys. B., 1: 365 (1968).
16. T. F. O'Malley, A. J. Cunningham, and R. M. Hobson. J. Phys. B., 5: 2126 (1972).
17. F. J. Mehr and M. A. Biondi. Phys. Rev., 176: 322 (1968).
18. Yueh-Jaw Shiu, M. A. Biondi, and D. P. Sipler. Phys. Rev. A., 15: 494 (1977).
19. Gerhard Herzberg. Molecular Spectra and Molecular Structure. (Van Nostrand Reinhold Company, New York, New York, 1950) pp. 392-393.

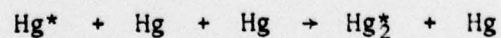
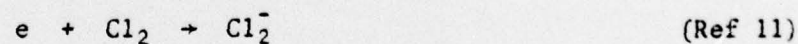
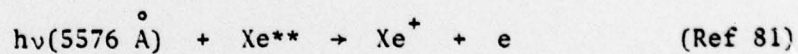
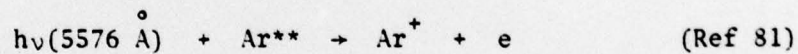
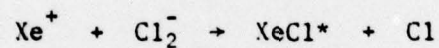
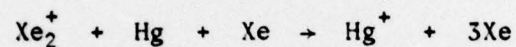
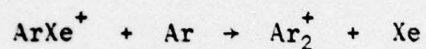
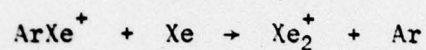
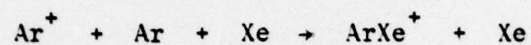
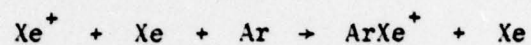
20. J. N. Bardsley and F. Mandl. Reports Prog. Phys., 31: 471 (1968).
21. T. L. Gilbert and A. C. Wahl. J. Chem. Phys., 55: 5247 (1971).
22. E. Schultes, A. A. Christodoulides, and R. N. Schindler. Chem. Phys. 8: 354 (1975).
23. G. D. Sides, T. O. Tiernan, and R. J. Hanrahan. J. Chem. Phys., 65 1966 (1976).
24. G. E. Caledonia. Chem. Rev., 75: 333 (1975).
25. D. C. Frost and C. A. McDowell. Can. J. Chem., 38: 407 (1960).
26. Bruce H. Mahan. J. Chem. Phys., 43: 3080 (1965).
27. B. M. Smirnov. Sov. Phys. JETP., 24: 1180 (1967).
28. Joseph O. Hirschfelder, Charles F. Curtis, and R. Byron Bird. Molecular Theory of Gases and Liquids. (John Wiley & Sons, Inc., New York, New York, 1954), pp. 983-989.
29. A. Dalgarno. Phil. Trans. Roy. Soc., A250: 426 (1958).
30. K. S. Pitzer. Quantum Chemistry. (Prentice-Hall, Inc., Englewood Cliffs, New Jersey, 1953), p. 339.
31. D. Smith, A. G. Dean, and I. C. Plumb. J. Phys. B., 5: 2134 (1972).
32. A. P. Vitols and H. J. Oskam. Phys. Rev. A., 8: 1860 (1973).
33. J. J. Thomson. Phil. Mag., 47: 337 (1924).
34. M. A. Biondi. Phys. Rev., 90: 730 (1953).
35. L. Schlie. Private communication.
36. G. Gioumousis and D. P. Stevenson. J. Chem. Phys., 29: 294 (1958).
37. D. K. Bohme, N. G. Adams, M. Mosesman, D. B. Dunkin, and E. E. Ferguson. J. Chem. Phys., 52: 5094 (1970).
38. D. Rapp and W. E. Francis. J. Chem. Phys., 37: 2631 (1962).
39. P. Langevin. Ann. Chim. Phys., 5: 245 (1905)
40. William B. Maier II. J. Chem. Phys., 62: 4615 (1975).
41. Earl W. McDaniel. Collision Phenomena in Ionized Gases. (John Wiley & Sons, Inc., New York, New York, 1964), p. 575.

42. J. M. Wadehra and J. N. Bardsley. Appl. Phys. Lett., 32: 76 (1978).
43. Earl W. McDaniel. Collision Phenomena in Ionized Gases. (John Wiley & Sons, Inc., New York, New York, 1964), p. 571.
44. Ibid, p. 19.
45. J. Sayers. Proc. Roy. Soc., A-169: 83 (1938).
46. Keith A. Brueckner. J. Chem. Phys., 40: 439 (1964).
47. G. L. Natanson. Sov. Phys.-Tech. Phys., 4: 1263 (1959).
48. M. R. Flannery. Submitted to Chem. Phys. Lett.
49. D. R. Bates and M. R. Flannery. J. Phys. B., 2: 184 (1969).
50. D. R. Herschback. Advan. Chem. Phys., 10: 319 (1966).
51. J. L. Magee. J. Chem. Phys., 8: 687 (1940).
52. J. E. Velazco and D. W. Setser. J. Chem. Phys., 62: 1990 (1975).
53. J. E. Velazco and D. W. Setser. IEEE J. Quant. Elec., 11: 708 (1975).
54. L. G. Piper, J. E. Velazco, and D. W. Setser. J. Chem. Phys., 59: 3323 (1973).
55. J. E. Velazco and D. W. Setser. Chem. Phys. Lett., 25: 197 (1974).
56. L. A. Gundel, D. W. Setser, M. A. A. Clyne, J. A. Coxon, and W. Nip. J. Chem. Phys., 64: 4390 (1976).
57. M. Schaper and H. Scheibner. Beit. Plasma Phys., 9: 45 (1969).
58. Stephen D. Rockwood. Phys. Rev. A., 8: 2348 (1973).
59. Walter L. Borst. Phys. Rev., 181: 257 (1969).
60. A. von Engel. Ionized Gases, 2 ed. (Oxford University Press, Oxford, 1965), p. 48.
61. J. C. McConnell and B. L. Moiseiwitsch. J. Phys. B., 1: 406 (1968).
62. L. Vriens. Private communication.
63. L. Vriens. Physica., 31: 385 (1965).
64. M. Gryzinski. Phys. Rev., 138: A336 (1965).
65. Arthur C. Jenkins and Gerhard A. Cook (Ed). Argon, Helium and the Rare Gases, Vol. I, (Interscience Publishers, New York, 1961), p. 237.

66. Gerhard Herzberg. Atomic Spectra and Atomic Structure, (Dover Publications, New York, 1944), pp. 201-202.
67. E. Bauer and C. D. Bartky. J. Chem. Phys., 43: 2466 (1965).
68. E. Bauer and C. D. Bartky. DDC No. AD627033, Aeronautic Report No. U-2943. January 1965.
69. M. A. A. Clyne and D. H. Stedman. Trans. Farad. Soc., 64: 2698 (1968).
70. E. Hutton and M. Wright. Trans. Farad. Soc., 61: 78 (1965).
71. L. W. Bader and E. A. Ogryzlo. J. Chem. Phys., 41: 2926 (1964).
72. G. A. Hart and S. K. Searles. J. Appl. Phys., 47: 2033 (1976).
73. T. H. Dunning and P. J. Hay. Appl. Phys. Lett., 28: 649 (1976).
74. M. J. Berger and S. M. Seltzer. NASA SP-3012 (1964).
75. D. Rapp and P. Englander-Golden. J. Chem. Phys., 43: 1464 (1965).
76. L. R. Peterson and J. E. Allen. J. Chem. Phys., 56: 6068 (1972).
77. Stanford Research Institute Report No. MP 76-99, (Stanford Research Institute, Menlo Park, California, December 1976).
78. C. H. Chen, J. P. Judish, and M. G. Payne. J. Chem. Phys., 67: 3376 (1977).
79. F. W. Lee and C. B. Collins. J. Chem. Phys., 65: 5189 (1976).
80. F. W. Lee, C. B. Collins, and R. A. Waller. J. Chem. Phys., 65: 1605 (1976).
81. K. J. McCann and M. R. Flannery. Appl. Phys. Lett., 31: 599 (1977).
82. A. Mandl. Phys. Rev. A., 3: 251 (1971).

APPENDIX A

Other Possible Reactions in the HgCl Laser



APPENDIX B

Photodetachment of Cl^-

The photodetachment of Cl^- is shown below.



This reaction is not included in this model because the cross section is zero at the 557.6 nm wavelength of the HgCl laser (Ref 82).

This zero cross section for the photodetachment of electrons from Cl^- indicates the HgCl photons are not at a higher energy than the threshold energy that is located at a wavelength of approximately 345.0 nm for this reaction (Ref 82).

Appendix C

M. R. Flannery's Ionic Recombination Curves (Ref 48)

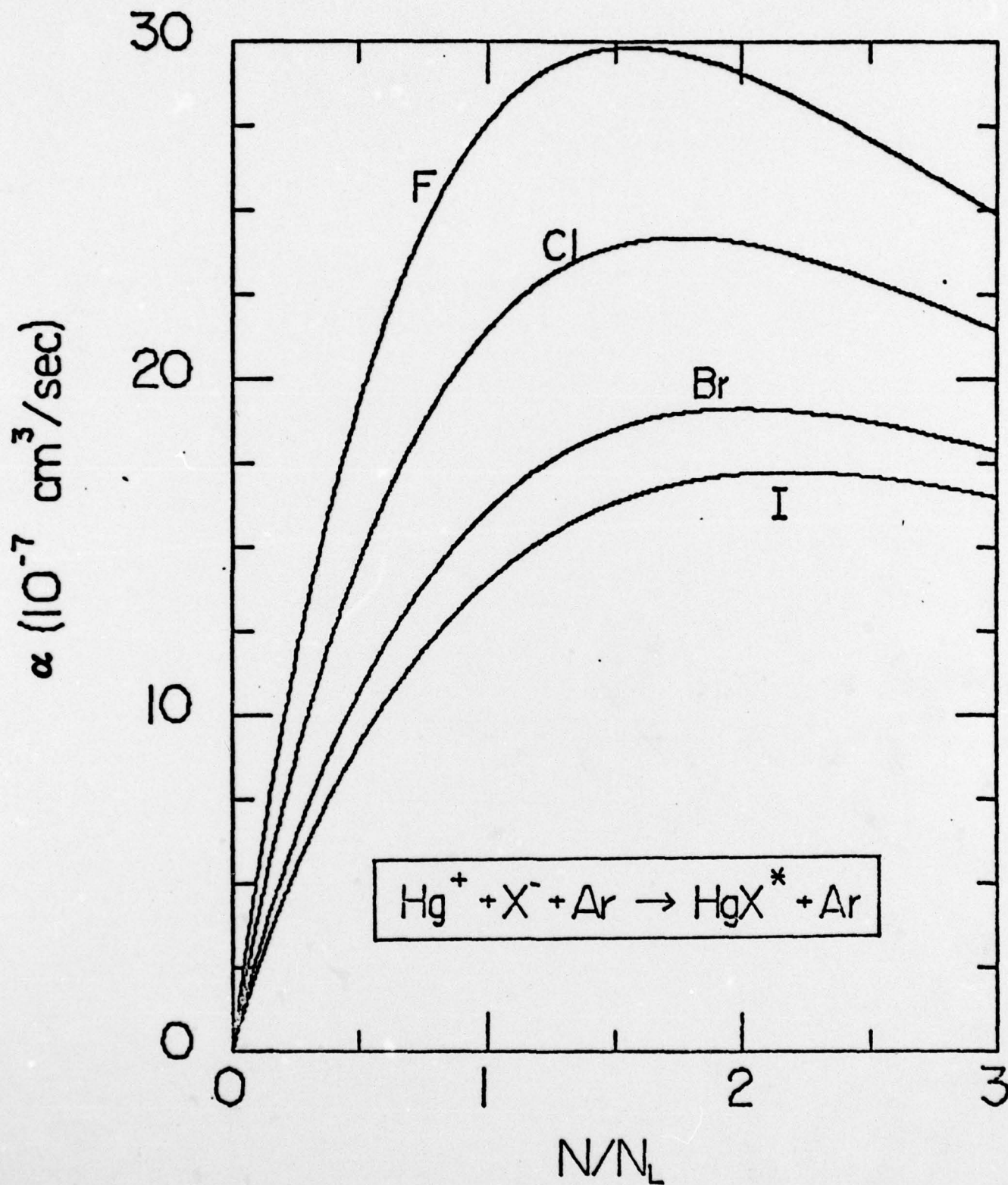


Fig. 10. Hg^+ and Cl^- Ionic Recombination Constants for Pressures to 3 Atmospheres (Ref 48)

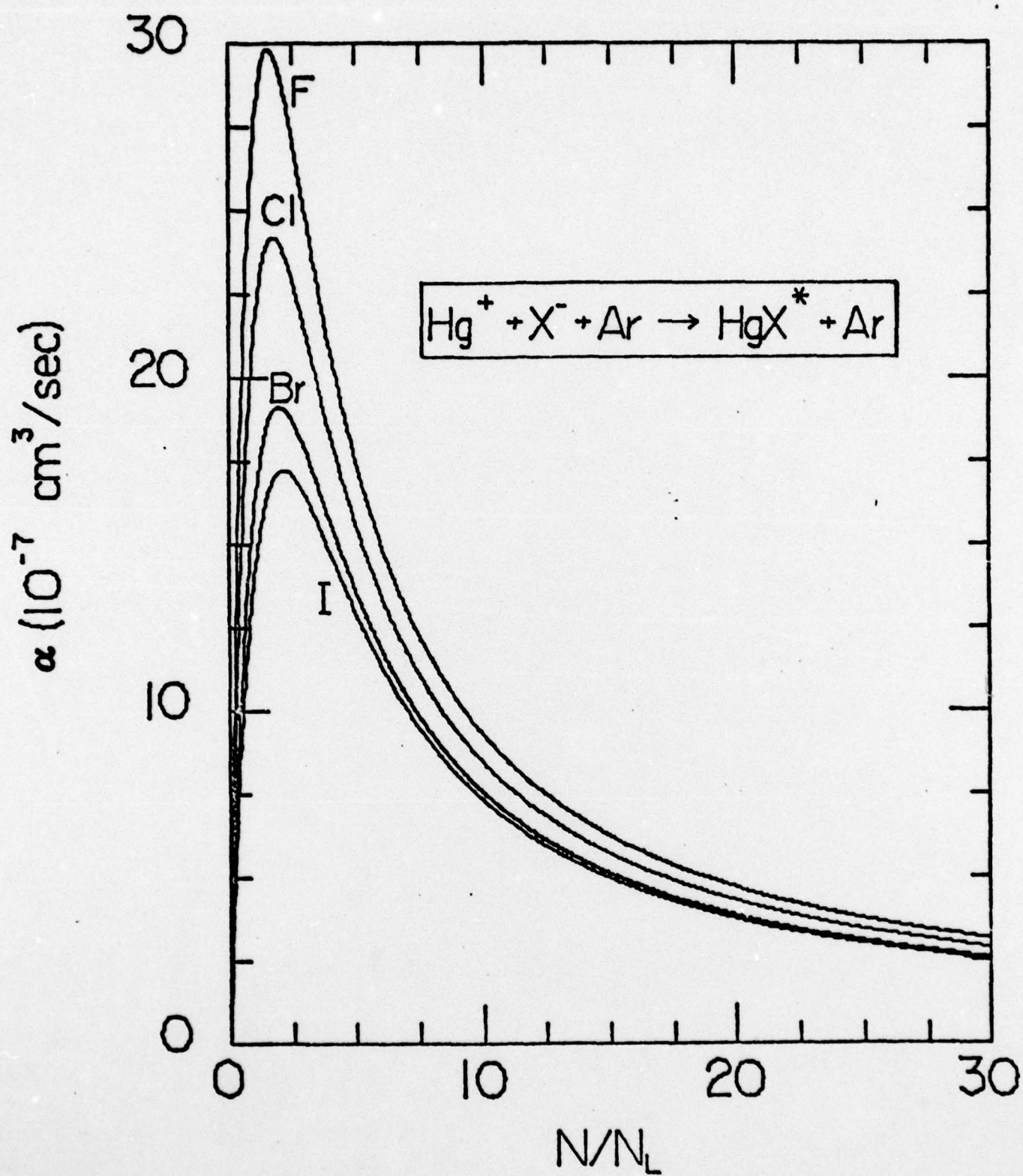


Fig. 11. Hg^+ and Cl^- Ionic Recombination Constants (Ref 48)

VITA

Robert P. Summers was born on 15 November 1949 in West Chester, PA. He is the son of Mr. and Mrs. Francis P. Summers of Downingtown, PA. He graduated from S. Horace Scott Senior High School, Coatesville, PA in 1967. He graduated from the U. S. Air Force Academy in 1973. He was a Deputy Missile Launch Officer and Deputy Missile Launch Officer Evaluator at Malmstrom AFB, MT until August 1976 when he entered the Air Force Institute of Technology.

Permanent Address: 4929 Purdue Ave NE
Seattle, WA 98105

This thesis was typed by Sharon Flores.

UNCLASSIFIED

SECURITY CLASSIFICATION OF THIS PAGE (When Data Entered)

REPORT DOCUMENTATION PAGE		READ INSTRUCTIONS BEFORE COMPLETING FORM
1. REPORT NUMBER AFIT/GNE/PH/78M-9	2. GOVT ACCESSION NO.	3. PERFORMING ORG. REPORT NUMBER
4. TITLE (and Subtitle) REACTION-RATE CONSTANTS AND SIMPLE RATE THEORIES APPLIED TO THE MERCURY-CHLORIDE LASER.	5. TYPE OF REPORT & PERIOD COVERED MS Thesis Master's thesis	
6. AUTHOR(s) Robert P. Summers Captain, USAF	7. CONTRACT OR GRANT NUMBER(s)	
8. PERFORMING ORGANIZATION NAME AND ADDRESS Air Force Institute of Technology (AFIT-EN) Wright-Patterson AFB, Ohio 45433	9. PROGRAM ELEMENT, PROJECT, TASK AREA & WORK UNIT NUMBERS	
10. CONTROLLING OFFICE NAME AND ADDRESS	11. REPORT DATE March 1978	12. NUMBER OF PAGES 117 P.
13. MONITORING AGENCY NAME & ADDRESS (if different from Controlling Office)	14. SECURITY CLASS. (of this report) Unclassified	
15a. DECLASSIFICATION/DOWNGRADING SCHEDULE		
16. DISTRIBUTION STATEMENT (of this Report) Approved for public release; distribution unlimited		
17. DISTRIBUTION STATEMENT (of the abstract entered in Block 20, if different from Report)		
18. SUPPLEMENTARY NOTES Approved for public release; IAW AFR 190-17 JERRAL F. GUESS, Captain, USAF Director of Information		
19. KEY WORDS (Continue on reverse side if necessary and identify by block number) Mercury-Chloride Laser Reaction-Rate Constants Laser Model		
20. ABSTRACT (Continue on reverse side if necessary and identify by block number) Several simple theories for reaction-rate constants are applied to the HgCl laser reactions. These theories are discussed and analyzed using existing data. The theories that are discussed are applicable to dissociative recombination, dissociative attachment, ion neutral association, bimolecular charge transfer, ionic recombination, and harpooning reactions. A simple theoretical model of the HgCl laser is constructed. The gases that are included in the laser are Ar, Xe, Hg, and Cl ₂ . Reaction-rate constants for the reactions are computed using either theoretical or experimental data. The model is analyzed using an analytical		

DD FORM 1 JAN 73 1473

EDITION OF 1 NOV 65 IS OBSOLETE

UNCLASSIFIED

SECURITY CLASSIFICATION OF THIS PAGE (When Data Entered)

012225

UNCLASSIFIED

SECURITY CLASSIFICATION OF THIS PAGE(When Data Entered)

approach and a computer generated solution. The model is found to be very sensitive to the dissociative attachment rate of Cl_2^+ and electron impact pumping rate constants. This report contains an 32-item bibliography.

UNCLASSIFIED

SECURITY CLASSIFICATION OF THIS PAGE(When Data Entered)